Geomorphic constraints on uplift history in the Aspromonte Massif, southern Italy

Gaetano Robustelli[1]

[1] Department of Biology, Ecology and Earth Science, University of Calabria (Italy).

E-mail, Corresponding author: gaetano.robustelli@unical.it,

Abstract

The landscape morphology of the Aspromonte Massif, southern Italy, shows hanging low-relief surfaces that correlate with uplifted landsurfaces which are preserved all around the massif. The drainage network has deeply incised the high-standing low-relief landscapes, seen here as being the remnants of phases of relief smoothing prior to strong uplift that has affected the area since the Middle Pleistocene. GIS-aided estimation of the rock volumes eroded since the late Early Pleistocene indicate high variability in denudation rates between the gently rolling landscapes and the river valleys. In this framework, longitudinal river profiles are examined for 42 river channels to constrain multiple non-equilibrium conditions and to reconstruct the long-term uplift history of the massif. Most profiles consist of three/four segments separated by knickpoints and suggest a complex incision pattern. Longitudinal profiles reveal two upper, low gradient channel segments, a zone of steep channels further down the low relief landsurface margin, and a very steep lower channel segment, particularly in the western quadrant. Upper channel segments correspond to the Relict Landscape (RLandscape – a high-standing landsurface on top of the massif) and the Hanging Landscape (HLandscape – a landsurface surrounding the RLandscape), respectively. Steeper middle and lower segments are the result of two-phase river incision that is linked to changes in regional uplift rates, and, subordinately, to rock strength properties. Indeed, analysis of river longitudinal profiles could indicate, initially, relatively slow Aspromonte uplift during the early Pleistocene and, then, pulses of rapid uplift during the Middle-Late Pleistocene. Multi-segment river longitudinal profiles are, therefore, evidence of the transient landscapes of Aspromonte in response to pulsed massif uplift.

Keywords: Channel longitudinal profiles; Landscape evolution; River incision; Aspromonte.

1. Introduction

Interaction between tectonics, climate and erosion has led researchers to search for mathematical models to analyse the evolution of the Earth's topography (Howard, 1994; Howard et al., 1994; Whipple and Tucker, 1999; Mayer, 2000) by extracting river landscape metrics from DEMs.

Although river systems are viewed as sensitive indicators of tectonic forcing on a landscape, channel profiles may have a typical concave-up shape despite rock uplift rates (Snyder et al., 2000; Kirby and Whipple, 2001). Whenever rivers experience steady and uniform tectonic, lithologic and climatic conditions, a dynamic equilibrium between uplift and erosion is established (Whipple, 2001; Willett and Brandon, 2002), generating smooth, concave-up and steady-state river profiles (Willgoose et al., 1991; Sklar and Dietrich, 1998; Whipple and Tucker, 1999). However, since base level changes and climatic signals are transmitted throughout the landscape (Howard et al., 1994; Whipple and Tucker, 1999, 2002; Ouimet et al., 2009), river networks may be in a transient state. In this respect, convexities or knickpoints are deemed as evidence for disequilibrium conditions (Snyder et al., 2000; Kirby and Whipple, 2001; Kirby et al., 2003; Molin et al., 2004; 2012; Schoenbohm et al., 2004; Wobus et al., 2006; Ouimet et al., 2009; Cyr et al., 2010, 2013; Olivetti et al., 2012).

Most of the stream-power family of incision models argue that bedrock incision is a function of drainage area and channel slope (Howard and Kerby, 1983; Seidl and Dietrich, 1992 Howard, 1994; Sklar and Dietrich, 1998; Stock and Mongomery, 1999; Whipple and Tucker, 1999, 2002). Longitudinal profiles of bedrock rivers may therefore yield valuable information about allocyclic mechanisms through variations in channel slope (e.g. Schoenbohm et al., 2004; Duvall et al., 2004; Wobus et al., 2006 and references therein). Indeed, slope-area analysis of channel profiles have served as important means of exploring landscape evolution and active tectonics in a number of studies (Snyder et al., 2000; Kirby and Whipple, 2001; Kirby et al., 2003, 2007; Schoenbohm et al, 2004; Ouimet et al., 2009; Weggmann and Pazzaglia 2009; Olivetti et al., 2012; Cyr et al, 2010, 2013).

In this paper, geomorphic and geologic data are combined with analysis of downstream changes in the longitudinal profiles of rivers draining the southern tip of the Calabrian Arc in order to understand aspects of Plio-Quaternary geomorphic evolution of the Aspromonte Massif. This approach may provide a useful tool with which to infer the long-term river response to external forcing and, particularly, spatial and temporal gradients in uplift rates. In this framework, low-relief landscapes, high variability in erosion rates, and reconstruct river profiles have allowed to constrain multiple non-equilibrium conditions which are useful to evaluate the history of Aspromonte uplift. Changes in the channel profile gradient of rivers draining the Aspromonte massif provide constraints on (i) the link between tectonics and landscape evolution in the region, and (ii) the role played by varying uplift, lithology and drainage area in geomorphic indices and knickpoint distribution.

2. Geological background of the Calabrian Arc

The Calabrian arc in the central Mediterranean (Fig. 1) is the product of different tectonic events relating to the formation of the Alpine Chain (Cretaceous-Paleogene), the Kabilo-Calabride Chain (Upper Oligocene–Lower Miocene), and the South-Apennine-Maghrebian Chain (Upper Miocene–Present) (Amodio-Morelli et al., 1976; Bonardi et al., 2001). It constitutes the forearc belt of the active subduction of the Ionian basin, which deepens to the northwest beneath the Tyrrhenian Sea (Amato et al., 1993; Piromallo and Morelli, 2003; Montuori et al., 2007).

Over the Neogene-Quaternary, the evolution of the Calabrian subduction zone is related to the subduction and trench rollback of the Ionian lithosphere which caused the opening of the Tyrrhenian basin and the formation of the Calabrian accretionary wedge (Malinverno and Ryan, 1986; Kastens et al., 1988; Patacca et al., 1990; Gueguen et al., 1998; Faccenna et al., 2001; Minelli and Faccenna 2010). As a result of the progressive increase in continental collision, the presence of lateral slab discontinuities and the ongoing decrease in the width of the trench induced slab breakup which led to clockwise rotation of the Calabrian belt (Van Dijk and Scheepers, 1995; Gueguen et al., 1998; Speranza et al., 2000; Faccenna et al., 2004; Chiarabba et al., 2008; Cifelli et al., 2008; Minelli and Faccenna, 2010)

During the Quaternary, the Calabrian Arc experienced extensional deformation that has resulted in the most impressive tectonic feature of the Calabrian Arc, the Siculo-Calabrian rift zone (SCRZ in Tortorici et al., 1995). This forms a N-trending fault belt of about 370 km in length that runs more or less continuously along the inner side of the Calabrian arc, extending through the Strait of Messina and along the Ionian coast of Sicily (Fig. 1). Many seismological, geodetic and structural data demonstrate that the SCRZ accommodates an almost uniform extension-rate of about 3.0 mm/yr along a ESE-WNW direction (D'Agostino and Selvaggi, 2004; Neri et al., 2005; Scarfì et al., 2007; Serpelloni et al., 2010).

This region experienced one of the most intense uplifts in the Mediterranean area during the Quaternary (Fig. 1) (Westaway, 1993; Miyauchi et al., 1994; Antonioli et al., 2006; Ferranti et al., 2006). In particular, late Quaternary uplift along with sea-level changes caused the development of flights of marine terraces (Valensise and Pantosti, 1992; Bordoni and Valensise, 1998; Dumas et al., 2000; Catalano and De Guidi, 2003; Ferranti et al., 2006; Bianca et al., 2011; Monaco et al., 2017).

2.1. Geologic setting

The Aspromonte Massif consists of a stack of nappes (Calabrian Arc Auct.) which include distinct tectonic slices of both crystalline terrains and Mesozoic–Cenozoic sedimentary sequences (Bonardi et al., 2001).

The basement units are composed of the remnants of both Variscan and Alpine metamorphic rocks (Bonardi et al., 2001; Pezzino et al., 2008). Three tectono-metamorphic units (Fig. 2) constitute the core of the massif. These are, from bottom to top and from north to south, the Lower Metapelite Unit, the Aspromonte Unit, and the Stilo Unit (Cirrincione et al., 2008).

Late Oligocene-Quaternary siliciclastic sediments (Fig. 2) up to 2000 m thick and deposited in the Ionian forearc basin unconformably overlie the pre-Cenozoic basement (Cavazza and Ingersoll, 2005). This sedimentary succession forms an overall E-dipping monocline characterised by a very apparent progressive unconformity, forming a wide range of homoclinal structures along the Ionian side of Aspromonte (Robustelli and Sorriso-Valvo, 2017).

The base of the forearc succession consists of discontinuous outcrops of conglomerates (Palizzi Fm.) and biocalcarenites (Pignolo Fm.) upon which the Stilo–Capo d'Orlando Formation (uppermost Chattian–Burdigalian) rests unconformably (Cavazza and Ingersoll, 2005); during this time span, fission track analysis show a phase of increased cooling rates relating to exhumation, crustal extension and subaerial erosion events (Thomson 1994a, 1994b, 1998). The Stilo–Capo d'Orlando Formation is composed of coarse and fine-grained deposits that are conformably overlain by the chaotic melange informally named ''varicolored clays'' (Cavazza and Ingersoll, 2005). A siliciclastic unit of Serravallian–Tortonian age composed of conglomerate, sandstone, and mudrock disconformably overlies the melange and passes upward to diatomaceous shales that are equivalent to the Tripoli Formation (Tortonian–Messinian boundary). The overlying Messinian siliciclastic deposits consist of a threefold succession that lies unconformably on the underlying sequence with an angular unconformity (Cavazza and DeCelles, 1998). The coccolith–foraminiferal marls of the Trubi Formation (Zanclean) onlap the Messinian deposits, as well as all older units, and indicate an abrupt change in sediment source; the Trubi Formation is paraconformably or disconformably overlain by a 200 metre thick succession (7 in Fig. 2) composed of weakly cemented sandstone and pelite passing to calcarenite sand-wave deposits (Calcareniti di Vinco Formation in Critelli et al., 2016, 2017a, 2017b).

Fission track analysis indicates little erosion during the Neogene-Quaternary (Thomson, 1994b), that is the present-day landscape is the result of the recent uplift of the belt. Indeed, a complex system of marine and alluvial terraced sediments discontinuously covers older formations. These terraces are found at elevations reaching to more than 1.000 m a.s.l., thus indicating a dramatic uplift of the Calabrian block over the last 700 ka (Tortorici et al., 1995). Furthermore, along the 80 km of coastline from Palmi to Melito di Porto Salvo (Fig. 1), fourteen marine terraces form a staircase between the present sea-level and 520 m a.s.l. (Dumas et al., 2000).

The foremost Quaternary tectonic feature of the region is the Siculo-Calabrian rift zone (Tortorici et al. 1995), a N-striking normal fault belt about 370 km in length that stretches along the inner side of the Calabrian arc as far as the Ionian coast of Sicily. This fault belt is made up of many segments, locally showing an *en-echelon* arrangement, that articulate the

Aspromonte Massif (Catalano et al., 2008). Many of the active segments exhibit apparent fault scarps that, on land, define the fronts of the Aspromonte Massif (Robustelli and Sorriso-Valvo, 2017) and, offshore, bound syntectonic basins. Although the seismicity of Calabria is among the highest in the whole of the Mediterranean, it is not well known on its Ionian side. However, Scarfì et al. (2009) indicate primarily a normal faulting mechanism along NE striking planes affecting eastern Aspromonte, which is consistent with the overall WNW–ESE extension direction also affecting the Straits of Messina (Del Ben et al., 2008; Scarfì et al., 2009; Polonia et al., 2012).

2.2. Geomorphologic setting

Aspromonte is a cone-shaped massif that rises from sea level to an average elevation of approximately 1,600 m a.s.l. at the highest plateau. Montalto is the highest peak (1,956 m) at a distance of only 20 km from the sea.

Noteworthy aspects include relics of landsurfaces hanging at elevations of between 500 and 1300 m a.s.l. and forming apparent step-like distributed landsurfaces around Aspromonte (Fig. 3). Albeit with some exceptions, the Ionian Aspromonte flanks decrease more regularly toward the Ionian Sea even though a segmented ENE-trending fault system is clearly apparent in the southeast. Instead, the landscape of the western side is highly influenced by the tectonic activity of the NE-striking normal fault belt (Figs. 2, 3) (Tortorici et al., 1995; Catalano et al., 2008; DISS Working Group, 2015; ISIDe working group, 2016; Rovida et al., 2016). This fault belt forms primarily west-facing, steep, straight fault scarps above which relics of the hanging landsurfaces, such as Piani d'Aspromonte, dominate the landscape (Robustelli and Sorriso-Valvo, 2017). These surfaces are considered to be stepped marine terraces of the Early Pleistocene (Miyauchi et al., 1994). However, scattered coverings of fluvial deposits with a similar degree of maturity affect most of relics, so suggesting that the landsurfaces in question could have partly developed through fluvial-denudational relief smoothing processes (Critelli et al., 2016, 2017a, 2017b; Robustelli and Sorriso-Valvo, 2017).

In the west, low-relief landscape patches are generally between 500 and 1350 m a.s.l., but average elevations are closer to 1000 m in the north (Fig. 3). These low-relief landsurfaces are best preserved in the west and in the north, but they can also be found in very discontinuous remnants in the east where they developed on a variety of rocks (Figs. 2, 3). Indeed, according to the lithology the landscape is shaped onto, the southern and eastern sectors show an undulating topography whose tops are locally characterised by thick saprolite horizons and Quaternary deposits (Calcaterra and Parise, 2010; Critelli et al., 2016, 2017a, 2017b). Here, NE-trending fault systems form high morphological scarps (Tripodi et al., 2018), the result of differential weathering and erosion.

The gently-rolling topography of the perched landsurfaces contrasts sharply with the deeply incised river network (Fig. 3). Rivers flowing into the Tyrrhenian Sea are short, steep bedrock rivers that flow straight and are approximately perpendicular to the coastline. Most rivers have their headwaters on the low-relief upland and are steep bedrock rivers in

their upper reaches, but one or more knickpoints separate them into a number of channel-segments. In the west and, particularly, in the south and east, low-gradient alluvial channels are typical of river lower reaches (called Fiumara in Sorriso-Valvo and Terranova, 2006). Hillslopes along the main rivers and in the tributary valleys are very steep, with frequent landslides and deep-seated mass-movement helped by rock mass strength and weathering (Greco et al., 2007; Calcaterra and Parise, 2010 and references therein).

The presence of widespread flights of marine terraces is characteristic of lower Aspromonte slopes (e.g. Dumas et al., 2000; Monaco et al., 2017). These are the result of interaction between tectonics and eustasy, and provide constraints for the late Quaternary uplift that the region experienced. In particular, raised marine shorelines associated with the MIS 5e high stand indicate non-uniform uplift rates (Fig. 1) moving eastward (Cosentino and Gliozzi, 1988; Valensise and Pantosti, 1992; Westaway, 1993; Miayuchi et al., 1994; Bordoni and Valensise, 1998; Dumas et al., 2000; Catalano et al., 2003; Ferranti et al., 2006; Bianca et al., 2011; Monaco et al., 2017). Moreover, Holocene beaches, terraces and tidal notches indicate an increase in short-term uplift- rates up to 2.2 mm/yr (Fig. 1) (Pirazzoli et al., 1997; Antonioli et al., 2004, 2006; Ferranti et al., 2007, 2008; Scicchitano et al., 2011).

3. Material and methods

3.1. Geomorphological analysis

A detailed geomorphological survey was performed with the aim of detecting landscape features of different types and ages. Geomorphological analysis focused on identifying gently rolling erosional and/or depositional landsurfaces as key elements for the reconstruction of the morpho-tectonic evolution of the Aspromonte massif and its uplift history. The combined use of topographic data, river profiles, slope and relief data, and aerial photographs was particularly useful for identifying low- and high-slope areas. Slope and elevation maps allowed identification of low-relief landscapes of less than ~10° in slope throughout the study area. Relative chronologies, altitudinal ranges and cross-cutting relationships between tectonic landforms and landsurfaces were used to group the relict landscapes into different orders. To better constrain the landscape evolution of the Aspromonte Massif, geological data (Critelli et al., 2016, 2017a, 2017b) were integrated with data derived from a geomorphologic analysis of the spatial and altimetric arrangement of relict landscapes. Age constraints on terraced landsurfaces were provided by morphostratigraphic correlations and regional considerations.

3.2. Long-term denudation rate

GIS-aided estimations of long-term denudation rate in river valleys have been attained through the reconstruction of gently rolling landsurfaces, following some approaches adopted in literature (Amato et al., 2003; Perez-Pena et al., 2009; Gioia et al., 2014). The methodology consists of reconstructing palaeotopography through analysis of the spatial and

altimetric distribution of the relics of an irregular surface prior to river entrenchment of the middle segment of river profiles as detected through the longitudinal profile analysis. Specifically, the aim is to quantify the erosion that occurred in the area after the shaping of the HLandscape (see section 4.1.) and its tectonic fragmentation (see section 4.1). The middle segment of longitudinal river profiles developed over a time span of about 400/500 kyr resulting in deep dissection of the HLandscape. Therefore, each relic or group of relating relics with similar degrees of maturity was extended to cover those fault scarps responsible for the displacement of the HLandscape relics. To do this, the landsurface relics were mapped, first by analysing topographic maps and aerial photographs and then by comparing and overlaying the polygons enclosing the best-preserved relics on slope maps obtained by a raster Digital Elevation Model (DEM) with a 20-m resolution. I thereby isolated the pixels (cells) representing the relics in question and excluded those pixels with slopes greater than 8°, as well as river valley-floor pixels. To reconstruct the presumed topography, the mapped relics were interpolated with a triangulated irregular network (TIN) that included all the relics of the upland landscape.

By comparing topographic profiles made for both present-day and reconstructed topography, the restored landsurface appears to account well for the relict landscape morphology. However, the erosion rates that were calculated likely contain a certain underestimation of denudational rate due to the possible presence of divide areas within the ancient landscape that might, therefore, not be included in the GIS interpolation.

The difference between the orographic volume from the modern topography and that underlying the reconstructed palaeotopography allows computation of the eroded volume. Its conversion to denudation rates was attained by dividing the eroded volume and the total area above the reference surface. Relative age constraints are obtained from integrating geological, geomorphological and longitudinal profile analysis data.

3.3. Longitudinal profile analysis

Bedrock river incision rate is expressed as a power law function of contributing drainage area and local channel gradient (Howard and Kerby, 1983; Sklar and Dietrich, 1998; Whipple, 2004). The change in height (dz/dt) over time of channel elevation depends on competition between uplift, U, and erosion, E, such that:

$$\delta z/\delta t = U - E = U - KA^{m}S \qquad (1)$$

where U is rock uplift rate, A is upstream drainage area (proxy for discharge), S is local channel gradient, K is a dimensional erosion factor dependent on lithology, climate, and sediment load, and m and n are positive constants related to basin hydrology, hydraulic geometry, and erosion process (Howard et al., 1994; Sklar and Dietrich, 1998; Stock and Montgomery, 1999; Whipple and Tucker, 1999, 2002; Snyder et al., 2000).

At steady-state landscape ($\delta z/\delta t = 0$), Equation (1) can be solved for equilibrium slope (S_e) (Tarboton et al., 1989; Sklar and Dietrich, 1998; Snyder et al., 2000):

$$S_e = k_s A^{-\theta} \quad (2)$$

where:

$$k_s = (U/K)^{1/n\,\theta} \quad (3)$$

$$\theta = m/n^{\theta} \quad (4)$$

The coefficients k_s and θ set the equilibrium channel steepness and channel concavity, respectively, and can be determined by regression of channel-gradient and drainage-area data (Wobus et al., 2006; Kirby and Whipple, 2012; Whipple et al., 2013 and referenced therein).

Detachment-limited models claim that a power law relationship exists between the steepness index and rock uplift rate, and that the concavity index (θ) is dependent on many factors, including erosion and rock uplift rates (Sklar and Dietrich, 1998; Howard, 1998; Snyder et al., 2000; Kirby and Whipple, 2001; Sklar and Dietrich, 2001; Whipple and Tucker, 2002; Tucker and Whipple, 2002; Duvall et al., 2004; Whipple, 2004; Wobus et al., 2006; Kirby and Whipple, 2012; Whipple et al., 2013).

Although theoretical considerations indicate that the concavity index (θ=m/n) spans a narrow range of values between 0.35 and 0.7, the observed values range from ~0.3 to 1.2 (Whipple and Tucker, 1999; Tucker and Whipple, 2002; Whipple, 2004). Many key factors influence the large range of observed concavity indices (Sklar and Dietrich, 1998, 2001; Howard, 1998; Kirby and Whipple, 2001; Roe et al., 2002; Tucker and Whipple, 2002; Whipple and Tucker, 2002; Whipple, 2004; Zaprowski et al., 2005). Indeed, moderate concavities (0.4–0.7) are associated with rivers equilibrated to uniform rock uplift. Low concavities (<0.4) suggest downstream increases in either incision rate or rock strength. High concavity indices (0.7–1.0) indicate downstream decreases in rock uplift rate or rock strength (Kirby and Whipple, 2001; Kirby et al., 2003). Extreme concavity values (negative or >1) are associated with abrupt knickpoints, and indicate marked differences in uplift rates and along-stream changes in rock erodibility (Duvall et al., 2004; Whipple, 2004; Schoenbohm et al., 2004; Hoke et al., 2007)

Equation (2) indicates that rivers equilibrated to tectonic and climatic conditions show a smooth longitudinal profile and no knickpoints. Changes in boundary conditions induce variations in the slope-area scaling that cause the development of a transient-state profile and abrupt changes in channel slope (knickzones and/or knickpoints). Although there is no full

understanding of fluvial incision processes (Whipple, 2004; Wobus et al., 2006; Kirby and Whipple, 2012; Whipple et al., 2013), knickpoints have been interpreted in terms of changes in either rock uplift rate or in rock strength. Hence, slope-area analysis of channel profiles is deemed a powerful qualitative tool for extracting information on tectonics, uplift and rock erodibility (Kirby and Whipple, 2001; Kirby et al., 2003; Duvall et al., 2004; Schoenbohm et al., 2004; Spagnolo and Pazzaglia, 2005; Wobus et al., 2006; Hoke et al., 2007; Haviv et al., 2010; Olivetti et al., 2012; Cyr et al., 2013; Andreani et al., 2014; Gioia et al., 2014; Andreani and Gloaguen, 2016; Roda-Boluda and Whittaker, 2016, 2017)

Hence, using a 20 m resolution DEM, longitudinal profiles were extracted for 42 river channels dissecting the Aspromonte Massif. Topographic data were extracted through the Stream Profiler Arc and MATLAB tool kit (Wobus et al., 2006; Whipple et al., 2007) to generate power law regression analysis of river slope against drainage area in log–log space. The resulting log S-log A diagrams yield estimates of the concavity (θ, the slope of the regression) and steepness indices (k_s, the regression y-intercept). Due to the great covariance of k_s with θ (Sklar and Dietrich, 1998), the steepness index was normalized (k_{sn}) using a reference concavity index of θ_{ref}= 0.45 (the same in Cyr et al., 2013) to compare streams from catchments of varying sizes (Wobus et al., 2006; Kirby and Whipple, 2012). In so doing, along-channel patterns of k_{sn} mark one or more channel segments separated by knickpoints, and provide a clearer picture of equilibrium or disequilibrium in river longitudinal profiles around the Aspromonte massif.

4. Results

4.1. Relict, hanging and terraced landscapes

The morphology of the Aspromonte massif, characterised by deeply incised low-relief landsurfaces, is a key issue in constraining surface uplift associated with development of these paleolandscapes. The Apromonte Massif shows a truncated cone-shape with flanks which are highly controlled by fault systems, showing very sharp rectilinear escarpments, and dissected by deep gorges that are considered the main geomorphic response to uplift. The low-relief landsurfaces of the study area can therefore be used as a datum to appraise tectonic influence on landscape evolution. In this respect, the rolling topography and the deep weathering mantle that characterise the low-relief surfaces reflect very different conditions from the rugged and uneven topography of the incised river valleys whose modelling is closely linked to tectonics, river and slope processes.

In order to distinguish the different conditions under which landscape developed, I use the name “Relict Landscape” (RLandscape) to refer to the low-relief upland landscape, “Hanging Landscape” (HLandscape) to refer to landsurface relics between 550 and 1300 m a.s.l. and “Terraced Landscape” (TLandscape) to describe the flight of marine terraces (Dumas et al., 2000) between the present sea level and 400 m a. s. l. (Fig. 4).

The top of the Aspromonte Massif consists of hanging relics of a low-relief, gently rolling landscape representative of the most ancient phases of relief smoothing. The RLandscape extends over an area >100 km^2 at an altitude exceeding 1400 m a.s.l. and exhibits a hummocky topography. This rolling topography alternates with low-sloping hanging valleys and wind gaps. Footslope cross-profiles appear concave and inclined by up to 20-25°. This landsurface is dominated by transport-limited erosion and has been markedly affected by weathering responsible for a great thickness of quartz-rich regoliths (Le Pera and Sorriso-Valvo, 2000; Calcaterra and Parise 2010; Greco et al., 2007; Robustelli and Sorriso-Valvo, 2017).

Although the lack of deposits prevents the determination of any chronological constraint, fission-track thermochronologic data indicate progressive exhumation through crustal extension and subaerial erosion between 25 Ma and 15 Ma (Thomson, 1994a, 1998). This was followed by the sedimentation of the Stilo-Capo d'Orlando Fm. (Cavazza and DeCelles, 1993; Cavazza and Ingersoll, 2005), whose basal strata indicate a palaeo-relief of ≥2 km (Thomson, 1994b). However, apatite fission-track data from the Stilo-Capo d'Orlando Fm. (Thomson, 1994b) coupled with other analytical techniques (Cavazza and Dahl, 1990) indicate a post-depositional re-heating between 10 and 5 My (late Miocene-Pliocene?), which matches well with tectonic and depositional events that occurred during the late Messinian (Cavazza and DeCelles, 1998). In this interpretation, it is assumed that the rear of the wedge experienced erosion leading to an earlier phase of relief smoothing. Hence, the RLaldscape is not older than late Messinian and is also consistent with regional considerations that indicate a Late Miocene-Pliocene age for the development of this gentle upland landsurface in the southern Apennines (Brancaccio et al., 1991; Amato and Cinque, 1999; Ascione and Cinque, 1999; Amato, 2000; Schiattarella et al.,, 2003, 2006; Ascione et al., 2012; Olivetti et al., 2012; Robustelli et al., 2014; Robustelli and Muto, 2017). Moreover, the age of the RLandscape can be constrained by stratigraphic data and their relationships with the lower HLandscape. Indeed, the HLandscape, in particular the relics which coincide with the Piani d'Aspromonte (Fig 4), certainly developed during the late Early Pleistocene as Calabrian sediments deposited on the HLandscape and lie unconformably on Piacenzian-Calabrian deposits (Calcarenini di Vinco Fm.; Fig. 1). The RLandscape is, therefore, undoubtedly older and its development must have occurred between the late Messinian and the Calabrian. However, some other matters need to be considered. After the Messinian, during the opening of the Vavilov back-arc basin (Kastens et al., 1988), the accretionary wedge experienced a forward propagation accompanied by uplift of the belt onto which Pliocene sediments were progressively deposited (Minnelli and Faccenna, 2010). During this time span, the onlap of the Trubi Formation (Zanclean) sealed all major pre-existing sedimentary accumulations, as well as the late Messinian fold and thrust structures (Cavazza and DeCelles, 1998). This reduced the land area and the terrigenous input to the basin (Cavazza and Ingersoll, 2005), yet the subsequent arkosic detrital component of the Calcareniti di Vinco Fm. (Monte Narbone and Calcarenites Fms. in Cavazza and Ingersoll, 2005) suggests a renewed erosion of the crystalline basement.

The Pliocene–Early Pleistocene deposits are, particularly, deemed to result from indentation of Calabria caused by the strike-slip and extensional tectonics responsible for the generation of WNW–striking palaeostraits that connected the Tyrrhenian area to the Ionian Sea (Tripodi et al., 2013; 2018), where the Calcarenite di Vinco Fm. was deposited during Piacenzian-Calabrian time span. The dominance of sandy deposits may support the possibility of a source area characterised by local relief in the order of a few hundred metres, but the presence of an older (late Messinian) low-relief landscape that has continued to weather, erode, and evolve cannot be ruled out. In any case, it is reasonable to assume that the RLandscape developed in the foregoing sedimentary scenario, during which fluvial-denudational relief smoothing processes (e.g. Amato and Cinque, 1999; Ascione and Cinque, 1999) also re-shaped the older, late Messinian paleolandscape. Therefore, the age of the RLandscape is constrained to Pliocene-Early Pleistocene, in agreement with age constraints provided by Schiattarella et al. (2013).

Moving downslope, the apparent N- to NNE-trending fault scarps of the Siculo-Calabrian rift zone (Tortorici et al., 1995) bound hanging remnants of low-sloping landsurfaces facing the sea between 500 and 1300 m a.s.l. (HLandscape in Fig. 4). The best example is the Piani d'Aspromonte, ranging in altitude from 900 to 1300 m a. s. l. The Hlandscape is widespread throughout the study area, even though mainly preserved in the north and northwest (Fig. 4). Here, in spite of the dearth of exposures, clastic deposits can be seen blanketing the landsurface locally. The overall effect is a smooth inselberg (the RLandscape atop Aspromonte) bounded by a piedmont low-relief landscape that is strongly dissected by a drainage network to the South. The origin of this inselberg is still being debated (Miyauchi et al., 1994; Robustelli and Sorriso-Valvo, 2017) and the depositional systems of the sedimentary cover are also as yet not well understood (Critelli et al., 2016; 2017a; 2017b), but the presence of both depositional and erosional surfaces suggests that the area experienced partial planation through relief smoothing processes (e.g. Amato and Cinque, 1999). In this interpretation, the RLandscape was surrounded by the slightly undulating topography (pediment) of the HLandscape, in agreement with the pre-existing relief invoked by Roda-Boluda and Whittaker (2017). This was the result of long-lasting erosional and depositional processes during long intervals of tectonic quiescence and developed during the Calabrian until it was displaced at different elevations across the active faults forming the Siculo–Calabrian Rift Zone (Tortorici et al., 1995). Clear step-like distributed surfaces were therefore scattered throughout the area between 500 and 1300 m a.s.l..

Downslope of the HLandscape, mid-Pleistocene uplift affected the study area is spectacularly documented by flights of marine terraces (TLandscape in Fig. 4). Along the 60 km of coastline from Scilla to Mèlito, fourteen marine terraces form a staircase between the present sea-level and 400 m a. s. l. (Dumas et al., 2000).

4.2. River Profile Analysis

Channel profiles of 17 river basins (Fig. 5) were extracted from digital topographic data. Linear regressions of the stream segments in slope-area plots allow the relative steepness (k_{sn}) and concavity (θ) indices reported in Table 1 to be found. Averaged data for each set of segments are presented for the entire drainage network and by quadrant (Table 2). The quadrants are (1) west and northwest of the Montalto summit (western side; Fig 4), within the core of the Siculo-Calabrian rift zone of Tortorici et al. (1995), and (2) east and southeast of the Montalto summit (eastern side).

Although the sample size is small, the concavity and steepness indices for the uppermost segments are rather uniform. The average concavity index for the 1st segment (0.34±0.20) falls within the range of commonly observed values (Tucker and Whipple, 2002), whereas the steepness index values are lower than 42 (Table 2).

Steepness and concavity from lower channel segments increase and, at times, show fair variability (Table 1). In particular, data analysis suggests (i) geographic variation in concavity index mostly for the 3rd segment, (ii) increasing steepness and concavity indices from the 1st to the 3rd segment, and (iii) significant variability in the 4th segment (Table 2). More precisely, the average concavity index for the 2nd channel segment (0.61 ± 0.27) also falls within the typically observed range (Tucker and Whipple, 2002). Average 3rd segment concavity indices are high (0.90 ± 0.35), but they decrease from northwest to southeast, whereas steepness index values are reasonably consistent among all segments (Table 2).

The rivers that drain the Aspromonte Massif exhibit a wide variety of profile forms (Fig. 6) that are very different from the equilibrium channel longitudinal profiles These profiles consist of two or more concave-up, knickpoint-bounded segments that were analysed according to their parameters and their position within each profile. Knickpoint elevations show three altitude ranges (300-500, 900-1300 and 1400-1650 m a.s.l.; Fig. 7). Field analysis indicates that many of the lower, minor knickpoints (not included in Fig. 7) facing to the SSW are undoubtedly affected by a number of lithologic contrasts.

River profiles show considerable similarities, even though they appear quite different at times. In general, the dominant profile form consists of two or three segments (Fig. 6). The segmented profile morphology is consistent with observations of the different landscapes characteristic of the study area. Longitudinal profiles that have no discernible or minor knickpoints, exhibiting an almost complete concave-up shape, are subordinate and concentrated in the West and in the south (Table 1).

Only 7 of the 17 river basins show an uppermost flat reach (1st segment) that stretches over the RLandscape with a low concavity index (<0.35 on average) and steepness index (<45 on average) (Table 2). These segments are bound downstream by a major knickpoint (Santagata, Bonamico 1, Laverde 1 and Catona 1 rivers in Fig. 6) that marks the edge of the upland RLandscape hanging over the gently sloping, sea-facing HLandscape.

For many profiles, the upper segment is absent, but minor knickpoints or convex channel segments are apparent (Gallico River in Fig 6). Upper segments (2nd) lie over the HLandscape with almost uniform concavity (mean $\theta \sim 0.61$) and low

steepness (mean k_{sn} ~ 61) indices (Table 2; Santagata, Catona1, Favazzina 1 and Laverde 1 rivers in Fig. 6). Middle segments are generally steeper and can contain small convex knickzones; the highest concavity (mean ~ 0.90) and steepness (mean~121) values are found in these segments (Fig. 6). Lower segments, except on the Tyrrhenian side, mostly reflect the transition between bedrock reaches and alluvial plains. These segments show high variability in concavity (from 0.37 to 3.8) and steepness indices (from 22.7 to 267). They are steeper and linear in the northwest with sharp convex knickzones marking their upper limits (Favazzina 1 and Sfalassà 1 rivers in Fig. 6). In the west and southeast, their variability and the presence of abrupt knickpoints are the result of evident along-stream changes in rock erodibility, where rivers cross alternating low and high erodible Late Oligocene-Quaternary siliciclastic sediments (Laverde 1 river in Fig. 6; Fig. 2) as well as transitions to fully depositional conditions (Table 2; Fig. 2).

4.3. Eroded volumes and denudation rates

For the calculation of average denudational rates, the timespan had to be chronologically constrained between the onset of the HLandscape dissection and of TLandscape development. This period is not easy to establish definitively, since it falls between the end the Early Pleistocene (Calabrian) and the Middle Pleistocene.

By correlating the average elevation of the 3rd knickpoint (430 m. a.s.l.) to that of marine terraces, the time interval between MIS 8.5 and MIS 9 (290-330 kyr; Dumas et al., 2000; Monaco et al., 2017) may postdate the dissection of the HLandscape.

As regards the HLandscape, it definitely developed during the middle-late Calabrian, being carved into the Calcareniti di Vinco Fm. (upper age limit between 1.2 and 1.7 Myr) and locally blanketed by clastic sediments (Critelli et al., 2016, 2017b). However, since the onset of the HLandscape dissection cannot be known precisely, the erosion rates were calculated for the minimum (~0.5 Myr) and the maximum values (~0.9 Myr) of the inferred age of dissection, considered not older than ~0.8 Myr (Early-Middle Pleistocene boundary) and ~1.2 Myr (uppermost age limit of the Calcareniti di Vinco Fm., respectively.

Fig. 8a shows altitude differences between the reconstructed paleotopography and the present-day topography.

GIS-aided analysis data of the study area indicate an average erosional downwearing of 157m. In particular the amount of erosion along river valleys is much higher on the Aspromonte massif flanks than on relict landsurfaces. Major river valleys show 450m and more of downcutting, particularly in the south and southeast.

The average erosion rate calculated since the dissection of the hanging landscape is $5.25 \times 10^5 m^3/yr$. In terms of downwearing, the average erosion rate is between 0.18 mm/yr^{-1} and 0.33 mm/yr^{-1}, depending on the age assigned to the beginning of the dissection of the HLandscape. The data gathered are quite consistent with the mean denudation rate in the Southern Apennines (0.22/0.30 mm/yr^{-1} in Amato et al., 2003; mean erosion rates of 0.23 mm/yr^{-1} in Martino et al.,

2009; 0,16/0,24 mm/yr^{-1} in Gioia et al., 2011) and along the southern and eastern slopes of Aspromonte (0.21 mm/yr^{-1} in Ibbeken and Schleyer, 1991), and are higher than mean denudation rates in the foreland of the Southern Apennine (0.03/0.15 mm/yr^{-1} in Gioia et al., 2014).

To compare the previous data with cosmogenic ^{10}Be erosion rate data provided by Cyr et al. (2013), the estimation of missing orographic volumes within river basins were also computed by removing hanging low-sloping areas just below the edge of Relict (R) and Hanging (H) Landscapes (Fig. 8b). The resulting mean denudation rate values are between 0.39 and 0.71 mm/yr^{-1} for the above quoted time interval and exceed 0.80 mm/yr^{-1} for the Amendolea River basin (Fig. 8c) if the minimum age of 0.5Myr is considered. High values of denudation rates along river valleys on the massif flanks suggest, therefore, low rates on low-sloping landsurfaces ranging from 0.045 and 0.082 mm/yr^{-1}.

Cosmogenic ^{10}Be erosion rates range between 0.62 and 2.01 mm/yr (Cyr et al., 2013) and match well the estimated short-term erosion rate data (from 0.9 and 2.7 mm/yr^{-1}) provided by Ibbeken and Schleyer (1991), which are higher than the long-term (1 Myr) mean erosion rates (0.21 mm/yr^{-1}).

As a whole, the time-independent topography of the study area and the faster erosion rates of the river valleys are consistent with a disequilibrium between uplift and erosion and suggest transient conditions of the Aspromonte massif. However, it can be reasonably assumed that the long-term model of denudation of the study area provides information on alternating periods of relief-smoothing processes and river dissection.

5. Discussion

Unlike equilibrium channel longitudinal profiles that reflect uniform and steady U and K, Aspromonte river profiles have marked convex knickpoints in their longitudinal profiles (Fig. 6). This apparent discontinuity in the slope-area data leads to a downstream increase in k_{sn} values. Indeed, local k_{sn} values show a clear pattern with respect to the elevation of channel segments and geographic variation within the study area (Table 2). Furthermore, Cyr et al. (2013) stated that high local k_{sn} values and high erosion rates are primarily the result of increased incision rates in response to higher uplift rates. Therefore, the Aspromonte massif becomes a key site for the investigation of landscape evolution through the analysis of the fluvial longitudinal profile morphology.

The local k_{sn} values of channels draining the Aspromonte Massif show a distinct spatial pattern and a good correspondence to active tectonic structures (Table 2, Fig. 9). The average normalized steepness of the uppermost channel segments shows low values, typically <45, whereas on the massif flanks, local k_{sn} values increase from ~63 to >100 (Tables 1, 2). These areas of different local k_{sn} are separated by prominent knickpoints (Fig. 6). Indeed, where river catchments show no changes in substrate erodibility, the erosion factor can be deemed spatially uniform. Consequently, the along-channel patterns of local k_{sn} values indicate that steeper channels result from increased incision rates in response to higher uplift

rates. In this sense, raised marine terraces provide the best constraint to evaluate long-term uplift rates (Cosentino and Gliozzi, 1988; Miayuchi et al., 1994; Bordoni and Valensise, 1998; Dumas et al., 2000; Ferranti et al., 2006; Bianca et al., 2011; Monaco et al., 2017), as high as 1.63 mm/y since the Middle Pleistocene on the western part of the Aspromonte massif.

The observed patterns of local k_{sn} which are similar to disequilibrium profiles in Cyr et al. (2013), are consistent with at least a four-stage channel evolution with knickpoints generated by unsteady rates of base-level fall. Indeed, the majority of river profiles exhibit three/four segments separated by two/three major knickpoints (Fig. 6). The uppermost segments that stretch over the relict landscape highest reach, located on the low-relief highest landsurface, are smooth, concave-up, have concavity indices of between 0.2 and 0.6 and low values of k_{sn} (see table 1 for averaged data). Moving downslope, a 1st knickpoint marks the change in channel slope and steepness index from the RLandscape to the low incised river segments dissecting the HLandscape. Steepness indices are still low (< 63), and concavity indices are between 0.2 and 0.9. The second stream profile segment (upper segment) shows a locally straight, concave-up profile and is bounded at the downstream end by the 2nd knickpoint, below which steepness indices are on average the highest in the study area. The 3rd segment has concavity indices of between 0.26 and 2.5. The 4th third stream segment (lower segment) shows a variable profile from a concave-up to straight or even convex-up shape, and has moderate steepness indices (~ 109) and concavity indices of between 0.55 and 3.8.

Therefore, river analysis indicates (i) a high mean concavity index (θ) for the lower channel segments (Table 1), and (ii) geographic variation in normalized steepness and concavity indices. The average concavity index for the first two segments, running over the Relict (0.34 ± 0.20) and Hanging (0.61 ± 0.27) Landscapes, falls within the range of commonly observed values (Tucker and Whipple, 2002). In the study area, the average normalized steepness index increases from the uppermost to the middle channel segments. To the east, the 3rd channel segment has the highest average normalized steepness index value, largely due to the contribution of the south-eastern sector. To the northwest, steepness and concavity index values for the middle and lower channel segments are the highest.

The average concavity index ($\theta = 0.34 \pm 0.20$) and normalized steepness index ($k_{sn} = 41.94$) for the uppermost segments are consistent with a relict landscape which developed during stable or slowly lowering base level conditions (Robustelli and Sorriso-Valvo, 2017; see section 4.1.). Beyond the upland surface (RLandscape), two or three major knickpoints are typical of river profiles. The 1st knickpoint marks a slight early change in channel slope and steepness index from the top of Aspromonte to the gently rolling landsurfaces of the HLandscape. Indeed, river profiles show an intermediate flat reach that stretches over the HLandscape, which is still marked by a low concavity index ($\theta = 0.61 \pm 0.27$) and a normalized steepness index ($k_{sn} = 61.46$). To the south, relics of this landscape become isolated because of river network dissection

(e.g. Piani di Bova and Mt. Scafi landsurfaces in Figs. 3 and 4). The 2nd knickpoint marks the abrupt change in channel parameters from the flat reaches (1st and 2nd channel segments) at a higher altitude to the deeply incised fluvial valleys. The onset of uplift-driven river incision triggered a regressive wave of incision that produced the abandonment of the HLandscape and the development of the 3rd channel segment (middle segment). The average steepness index values are basically the same throughout the study area, and contrasts with variability in concavity indices (Table 2). These values are highest in the northwest.

Several factors are believed to influence the variability in the concavity index in natural streams (Kirby and Whipple, 2012; Whipple et al., 2013 and references therein). Given that the middle segments run across the HLandscape, which is tectonically fragmented by fault systems of the Siculo–Calabrian Rift Zone, it is reasonable to assume that differences in the concavity of middle segments is the result of downstream change in rock uplift rates, primarily in the western quadrant (Kirby and Whipple, 2001; Whipple, 2004; Schoenbohm et al., 2004; Hoke et al., 2007). However, the high mean values of the concavity index may also reflect adjustments in the channel gradient in response to spatial variations in substrate erodibility (Whipple and Tucker, 1999, Kirby and Whipple, 2001; Sklar and Dietrich, 2001; Whipple and Tucker, 2002; Duvall et al., 2004; Whipple, 2004). Differences in rock erodibility from the study area, mostly in the south and southeast (Fig. 2), provide confirmation of this interpretation. In this regard, if channel segments with lithologic contrasts are excluded, concavity values are between 0.5 and 0.7, hence within the range of steady state profiles. River segments flowing from resistant (Aspromonte unit) to less resistant (Lower Metapelite unit) exhibit the highest concave profiles (e.g. Duvall et al., 2004)

Another key observation is geographic variation in both the normalized steepness index and the concavity index for the lowermost channel segments. Channels are steepest to the north of Aspromonte and become less steep when moving anticlockwise. Variations in the channel steepness index may reflect different uplift conditions, as this is consistent if one compares long-term uplift rates to steepness indices. Indeed, the highest values of the steepness index are in the northwestern quadrant, where uplift rates increase from 1 to 1.4 mm/yr^{-1} (Ferranti et al., 2006; Monaco et al., 2017). In the west, uplift rates are as high as 1.31 mm/y r^{-1}, and then decrease as we move eastward to as low as 0.63 mm/yr^{-1} (Cosentino and Gliozzi, 1988; Miayuchi et al., 1994; Bordoni and Valensise, 1998; Dumas et al., 2000; Ferranti et al., 2006; Monaco et al., 2017). However, there are some other matters that need to be considered in terms of the role of lithology in determining the channel steepness index. Many of the segments facing the Tyrrhenian Sea dissect the Aspromonte Unit (amphibolite facies metamorphic rocks intruded by granitoid bodies; Cirrincione et al., 2008) and are capable of supporting steep channels. Farther east, the influence of high erodibility bedrocks is clearly noticeable (Stilo and lower Metapelite Units in Cirrincione et al., 2008: metapelite, from low-greenschist to lower amphibolite facies metamorphic rocks; Oligocene-Quaternary sediments of the Ionian forearc basin in Cavazza and Ingersoll, 2005), and

channel steepness indices are lower accordingly (Tables 1, 2). As further support for this, the steepness index values decrease markedly in the southeast (Table 2) where Varicoloured Clays Fm. (a melange composed of thinly bedded red, greenish, and bluish clays enclosing beds of quartzarenite and limestone; Cavazza et al., 1997) extensively outcrops.

Regarding the concavity index, a range of perspectives may account for the variability of lowermost channel segments (Schoenbohm et al., 2004; Kirby and Whipple, 2012; Whipple et al., 2013). Since the lithology is fairly uniform to the northwest, temporal and spatial variations in uplift rate may influence the concavity index (Whipple and Tucker, 1999; Schoenbohm et al., 2004; Whipple, 2004). Indeed, if uplift rates decrease with time (e.g. Monaco et al., 2017), channel segments formed earlier will be steeper than later-formed channel segments, thus resulting in high concavity index values (Table 2). However, the rectilinear to convex profiles of the Sfalassà 1 and Favazzina 1 lower segments (Fig. 6) indicate that fluvial dissection does not keep up with uplift rates, as uplift rates increased in the Late Pleistocene-Holocene (Antonioli et al., 2004, 2006; Ferranti et al., 2007). Moreover, the southward increase of late Pleistocene and Holocene uplift rates (Ferranti et al., 2007 and references therein) match the variability in concavity index values between Palmi and Villa S.Giovanni quite well.

Although climate can be a key factor in channel geometry (Hijmans et al., 2005; Wobus et al., 2006; DiBiase and Whipple, 2011; Champagnac et al., 2012; Bookhagen and Strecker, 2012), D'Arcy and Whittaker (2014) argued that southern Calabria lacked the orographic coupling of elevation with the precipitation rate signal. This results in uplift rate having a great influence upon channel geometry, and particularly on the steepness index.

Along the western flank of Aspromonte, the average value of the concavity index is still high (1.41 ± 0.37). Although high concavities depend on a number of factors (Kirby and Whipple, 2012; Whipple et al., 2013), along-stream changes in substrate properties (e.g. Duvall et al., 2004) and the extent of the river bed alluvial cover (e.g. Sklar and Dietrich, 2004, 2006) are the key factors for increasing in-channel concavity.

To the south and southeast, poor outcomes arise from the power-law regression analysis of river slope against drainage area because of the stepped profile of lowermost segments due to the apparent along-stream changes in lithology and the extent of the river bed alluvial cover. However, it is noteworthy that some channels (Elia 2, Elia 3, Elia 4 and Palizzi 1 in Table 1) showed equilibrium channel longitudinal profiles that reflect uniform and steady U and K, even though minor knickpoints in longitudinal profiles occur. Moreover, some river segments flowing from resistant to less resistant bedrock (Bruzzano 1; Careri 1 and 2 in Table 1) exhibit highly concave profiles.

5.1. Aspromonte Uplift and River Incision

The existence of gently rolling landscapes at high elevations is a remarkable clue to the significant surface uplift of their margins. These step-like distributed surfaces also indicate that relief dismantling was discontinuous and characterised by

alternating phases of downcutting and of base-level stability; the role of climate changes is considered to be secondary because in mountainous areas close to the sea such variations have minor influence on aggradation and/or dissection (Robustelli et al., 2005 and references therein). Indeed, as changes in tectonic forcing appear to be responsible for slope-break knickpoint development (Kirby and Whipple 2012; Whipple et al., 2013), the three/four-segment river morphology of the study area (Fig. 6) could be the result of pulsed surface uplift affecting the Aspromonte uplift. Therefore, river profile analysis together with hanging remnants of gently rolling landsurfaces and geological data provide constraints for reconstructing the main stages of landscape evolution of the Aspromonte Massif.

Despite some uncertainty about the timing of the onset of Aspromonte geomorphological history (see section 4.1.), it can be reasonable assumed that the RLandscape developed during the Piacenzian-Calabrian time span (Fig. 10). It was the result of fluvial-denudational relief smoothing processes acting during a period of relative stability in the erosional base-level, which led to the development of concave-up, low gradient footslopes and shallow-sloping valleys. The highest channel segment of longitudinal river profiles and the presence of low-relief landscape atop Aspromonte suggest the most ancient phase of relief smoothing, contrary to the claim of Pirrotta et al. (2016).

In the subsequent stage, uplift rate increased, caused isolation of the uppermost channels and allowed the development of the 1st knickpoint and the upper concave-up river profile segments. (Fig.10). Despite the unclear marine or continental origin of clastic sediments locally blanketing the HLandscape, the upper segment of longitudinal profiles appears well-graded to this landsurface. The age of clastic sediments allows us to limit the formation of the relict landscapes to the late Early Pleistocene (Calabrian). What is more, it also provides time constraints on the main dissecting phase and, very importantly, predates the active faulting that took place during the Middle-Late Pleistocene (e.g. Roda-Boluda and Whittahker, 2017), in the context of the crustal extension which produced the so-called Siculo-Calabrian rift zone (Tortorici et al., 1995; Monaco and Tortorici, 2000; Catalano et al, 2008).

Indeed, the Middle Pleistocene marks a significant change in the geomorphological scenario of the study area. The ESE–WNW trending regional extension allowed the development of the Siculo-Calabrian Rift Zone (Tortorici et al., 1995), the major Late Quaternary tectonic feature of the Calabrian Arc that outlined the shape of the massif. The SCRF caused the most significant and marked vertical fragmentation of the HLandscape, and reduced the width of the massif, especially to the northwest (Fig. 10). In this regard, by considering the analogous degree of maturity between the lower (Piani della Melia, Solano and Vermeni) and the higher (Piani d'Aspromonte) relics of the landsurface in question (Fig.3), and similar associated deposits on both downthrown and raised blocks, it would appear that the NE-trending S. Eufemia-Calanna Fault (Fig. 3) was responsible for an offset of up to about 500 m. During this period, extensional tectonics created horst-and-graben structures with N-S and NE–SW trends (Capo Vaticano, Serre and Aspromonte highs; Mesima, Gioia Tauro, Reggio Calabria and Siderno basins; Tortorici et al., 1995). While grabens suffered marked subsidence, horst structures

underwent uplift and river dissection, and a marked increase in the local relief took place accordingly. Due to dissection, large volumes of bedrock were dismantled, leading to the development of the thick epiclastic Middle Pleistocene successions (Ghisetti, 1984; Barrier, 1986; De Rosa et al., 2008; Carbone et al., 2008; Di Stefano et al., 2007; Di Stefano and Longhitano, 2009; Critelli et al., 2016; 2017, 2017a).

It was within this framework that the isolation of the upper river segment and the development of the concave-up middle channel segment took place. High concavities of the middle-segment (the average value is between 1.12 ± 0.36, in the West, and 0.80 ± 0.34, in the East; table 2) may suggest declining uplift rates with time (e.g. Whipple and Tucker, 1999; Schoenbrohm et al., 2004). This claim appears consistent with the decreasing subsidence rates of marine basins (Reggio Calabria, Siderno, and Mesima), leading to their sedimentary filling (e.g. Ghiaie e Sabbie di Messina Fm. in Carbone et al., 2008), and with the evolution of the Catona and Petrace rivers as well (Pirrotta et al., 2016). It, therefore, may place the end of this phase in the late Middle Pleistocene, and predates the development of Middle-Late Pleistocene flights of marine terraces (I to VI order in Monaco et al., 2017) carved into the above mentioned gravel and sand deposits (Fig. 10). Furthermore, there are some other matters that need to be considered since the age of the onset of marine terracing is still being debated (Westaway, 1993; Miyauchi et al., 1994; Dumas et al., 2000; Catalano et al., 2008; Monaco et al., 2017). Firstly, due to the strong vertical fragmentation of the HLandscape (e.g. Roda-Boluda and Whittaker, 2017), the downthrown blocks (Piani della Melia, Solano and Vermeni landsurfaces in Fig. 3) experienced further reshaping by subaerial processes, as suggested by the presence of conglomerate and sand cover, which is locally overprinted by pedogenetic features. Secondly, the silt and reddish sand cover of the highest terraces (VII to X order in Monaco et al., 2017; TM290 to TM510 order in Dumas et al., 2000) allow us to reinterpret them as having partly developed during periods of subaerial landscape modelling. Moreover, cross-cutting relationships between tectonic landforms and flat lying surfaces (VII to X order in Monaco et al., 2017) help us to argue that some switches between aggradation or degradation occurred during the late Middle Pleistocene, up until the filling of sedimentary basins. Indeed, biostratigraphical and geomorphologic data in the Straits of Messina area (Catalano and Cinque, 1995; Catalano and Di Stefano, 1997; Carbone et al., 2008) suggest a complex depositional architecture of the Reggio Calabria basin fill resulting from the interplay of tectonics and eustatically induced base-level changes.

Clearly, more data are needed before a reliable comparison of terracing and stream profile development during the late Middle Pleistocene can be made. However, the relict profile was reconstructed by projecting the middle river segment downstream (Fig 11), following the suggestions of Andreani et al. (2014) and Andreani and Gloaguen (2016). The projection of the relict profile provides a measure of the surface uplift and of its starting age by finding the correspondence between flat morphological surfaces and the modeled river profiles. To do this, the middle segments of Catona 1 and 2 were chosen and modeled because terraced surfaces (Dumas et al., 2000; Pirrotta et al., 2016; Monaco et al., 2017) are

best preserved between Catona and Gallico. Projection of the middle segments of the Catona River (Fig. 11) appears quite well-graded to the elevation of VII/VIII terrace orders by Monaco et al. (2017), which corresponds to TM 290/TM320 by Dumas et al. (2000). Based on absolute dating provided by Balescu et al. (1997) and correlation between terraces and high stands of the eustatic curve (Dumas et al., 2000), the age that predates the further abrupt increase in uplift rate, which generated the 3rd knickpoint and the lower channel segment, is robustly limited to being between 200kyr (MIS 7.1) and 290kyr (MIS 7.5). In this interpretation, tectonics had a marked influence on accommodation space for the deposition of the Reggio Calabria Basin fill and the Ghiaie e Sabbie di Messina fm. Therefore, during the late Middle Pleistocene, regional uplift was not counterbalanced by hanging-wall subsidence in the Reggio Calabria and Armo faults as argued by Roda-Boluda and Whittaker (2017).

The youngest stage of landscape evolution is the flight of marine terraces down from 300m a.s.l., partly carved onto the previous clastic successions. The estimated uplift rates range from 0.8 to 1.7 mm/yr (Westaway, 1993; Dumas et al, 2000, Valensise and Pantosti, 1992, Monaco et al., 2017), even though Dumas et al. (1988) refer to an accelerated uplift between 140-115 kyr Similarly, Catalano et al. (2003) account for a significant change in uplift rates from 3.7 mm/yr (125-100 kyr) to 1-1.1 mm/yr (100-60 kyr). Recent dating of raised Holocene shorelines (Antonioli et al., 2006; Ferranti et al., 2007) indicates that uplift rates increased from 1.3 to 2.1 mm/yr from the late Pleistocene to the late Holocene: indeed, Ferranti et al. (2007) argue that uplift rates changed over time during the Late Pleistocene. Despite the preceding survey, a new increase in uplift rates caused the development of the 3rd knickpoint and the lowermost river profile segment (Fig. 10). The rectilinear to convex profiles of some segments facing the Tyrrhenian sea (Favazzina1 and Sfalassà 1 channel segment; Fig 6) suggest an imbalance between uplift and erosion.

Fault activity accompanying the last phase of uplift increase relates locally and markedly to the spatial distribution of the steepness index. Indeed, rivers facing to the northwest suggest that a clear and consistent tectonic influence is responsible for local convexities and increase in the steepness index (Table 1). In the west, though the activity of the NE- and WNW-striking fault systems is well constrained (Ghisetti, 1992; Monaco and Tortorici, 2000; Catalano et al., 2008), the role of lithologic controls is believed to produce an average decrease in the steepness index that significantly diminishes as we move anticlockwise to the southeast. Similarly, the wider range of the concavity indices from the west to the southeast (table 2) reflects significant along-stream changes in lithology as well as the extent of alluvial cover of the bed (Duvall et al., 2004; Sklar and Dietrich, 2004, 2006, Kirby and Whipple, 2012; Whipple et al., 2013). Indeed, alluvial floodplains (Sorriso-Valvo and Terranova 2005) are widespread to the west and, particularly, to the south and east.

Analysis of knickpoint elevations around the Aspromonte massif shows different spatial patterns. The 2nd knickpoint elevation (Figs. 12a, 12 b) increases roughly linearly from the northwest as we move anticlockwise around the Aspromonte massif, whereas elevations of the 3rd knickpoint exhibit an undulatory pattern (Fig. 12c), reaching a

maximum elevation along the western and southeastern flanks of the Aspromonte. Although bedrock incision models argue that the vertical knickpoint velocity is constant (Niemann et al., 2001; Kirby and Whipple, 2012), a range of perspectives influences the variability in knickpoint elevation and retreat rate (Hayakawa and Matsukura, 2003; Bishop et al., 2005; Berlin and Anderson, 2007; Haviv et al., 2010). As regards the spatial and vertical distribution of the 2nd knickpoint, its geographic variation appears to match the progressive increase in rock erodibility quite well due to the increasing presence of Late Oligocene-Quaternary sediments and the Lower Metapelite Unit (Fig. 1). Furthermore, variations in the 2nd knickpoint distribution also appear to depend on changes in the drainage basin area, with many of the largest basins located above the regression line. The undulatory pattern of the 3rd knickpoint may indicate that differential uplift influenced the distribution of knickpoint elevations (e.g. Olivetti et al., 2012), as no significant influence emerges from rock strength properties and the drainage area. To the northwest, the maximum elevation matches the highest middle-late Pleistocene uplift rates (Valensise and Pantosti, 1992; Bordoni and Valensise, 1998; Dumas et al., 2000; Ferranti et al., 2006; Monaco et al., 2017) and the activity of the Scilla, Reggio Calabria and Armo fault systems (Ghisetti, 1992; Tortorici et al., 1995; Monaco and Tortorici, 2000; Catalano et al. 2008). The high average knickpoint elevation in the southeast, for which no uplift data are available (Fig. 1), could indicate the role played by the NE-striking fault systems (Capo Spartivento faults in Figs. 3, 9). Based on the above statements, the role of tectonic uplift is believed to be still noticeable over short timescales (up about 400-500 kyr), but over long timescales (> 800 kyr, the upper age limit of the HLandscape dissection), rock strength properties and drainage area appear to be the key factors on knickpoint distribution. In summary, the Aspromonte Massif experienced non-uniform or unsteady regional uplift overlapping by local tectonics. The hypothesis of this type of uplift is primarily supported by (i) the presence of two orders of gently rolling landscapes that belong to uncompleted cycles of erosion that occurred during the Aspromonte uplift, and (ii) the segmented nature of many river profiles. In particular, the 2nd knickpoint and the related HLandscape mark the rapid onset of uplift-driven river incision. River profile morphology is driven by changes in the uplift rate over time, while climate control is ruled out. As an interesting side note, some key factors influence the distribution of knickpoint elevations. The 2nd knickpoint migration rate is sensitive to rock erodibility and drainage area, while the rectilinear to convex profiles of the lower segment in the western quadrant suggest that erosion does not balance rock uplift during the late Middle Pleistocene-Holocene.

6. CONCLUSION

Relict landscapes (erosional and/or depositional surface) and raised marine terraces have served as important markers of tectonic uplift in the study area, which underwent the most marked regional uplift in southern Italy. Given that drainage systems can be very sensitive to variations in rock uplift rates, Aspromonte has been a suitable site to investigate the

effects on the spatial distribution of bedrock channel gradients, assess the uplift history of the massif and improve knowledge of Quaternary landscape evolution along this margin of the Southern Apennines.

In this paper, two low-relief landscapes in the study area are described: Relict and Hanging Landscapes. The HLandscape is quite continuous and well developed along the western margin of Aspromonte. These landscapes developed under nearly stable base-level conditions. Both landscapes are cut by the active fault systems of the Siculo-Calabrian rift zone and are deeply incised by the drainage network. Rivers record two phases of river dissection since the Early-Middle Pleistocene boundary and tectonic deformation of the region, including ~1000 m surface uplift.

In this context, morphometric analysis of hydrography has been performed, along with the estimation of mean denudation rates during the late Early-Middle Pleistocene, which are higher on the flanks of the Aspromonte massif (up to 0.71 mm/y^{-1} in average). Analysis of stream longitudinal profiles reveals (1) a three/four-segment channel morphology for most rivers, (2) high mean steepness (k_s) and concavity (θ) index values for the middle and lower channel segments, respectively, and (3) geographic variation in steepness (k_s) and concavity (θ) indices. The highest reaches (1st and 2nd segment), stretching over the R and HLandscapes, are concave-up and characterised by low average values of steepness index and average concavity indices. The 2nd knickpoint marks the edge between the gently rolling landscapes and the Aspromonte flanks. The highest steepness indices (middle and lower segments) are spatially associated with the flanks of the massif, but channel profile concavity throughout the study area appears to be partly related to the steepness index. The steepening appears to be locally dependent upon uplift rates, but differences in concavity indices yield information about rock erodibility and the extent of alluvial cover.

Variable rates of knickpoint migration may have locally overtaken the upstream knickpoints, thus contributing to the presence of rivers with fewer channel segments. Analysis of knickpoint elevations indicates that their spatial and vertical distributions depend on a variety of key factors. What is more, the variability in knickpoint elevation and geographic distribution has proved to be a useful tool for understanding the timescale of landscape response to rock uplift (shorter timescale) or to rock strength properties and drainage area (longer timescale).

Differences in the amount of erosion between river valley and low-relief landsurfaces, and disequilibrium longitudinal profiles indicate a transient landscape where the three/four channel segment morphology can be simply interpreted as the result of pulsed surface uplift: relatively slow uplift during the development of gently rolling landscapes, then pulses of rapid uplift during the third (Middle Pleistocene) and fourth geomorphological evolutionary stage (since late Middle Pleistocene).

ACNOWLEDGEMENT

I thank Francesco Muto and Vincenzo Tripodi (University of Calabria) for useful discussions on the study area. I would like to thank Martin Brimble, who kindly revised English. The author would like to thank two anonymous reviewers for improvements to the manuscript.

References

Amato, A., 2000. Estimating Pleistocene tectonic uplift rates in the southeastern Apennines (Italy) from erosional landsurfaces and marine terraces. In: Slaymaker, O. (Ed.), Geomorphology, Human Activity and Global Environmental Change, John Wiley and Sons Ltd., 67-87.

Amato, A., Alessandrini, B., Cimini, G., Frepoli, A., Selvaggi, G., 1993. Active and remnant subducted slabs beneath Italy: Evidence from seismic tomography and seismicity. Ann. Geofis. 36, 201– 214.

Amato, A., Cinque, A., 1999. Erosional land surfaces of the Campano-Lucano Apennines: genesis, evolution and tectonic implications. Tectonophysics 315, 251–267, doi: 10.1016/S0040-1951(99)00288-7.

Amato. A., Aucelli, P.P.C., Cinque, A., 2003. The long-term denudation rate in the Southern Apennines Chain (Italy): a GIS-aided estimation of the rock volumes eroded since middle Pleistocene time. Quat. Int. 101–102, 3–11, doi.org/10.1016/S1040-6182(02)00087-3.

Amodio-Morelli, L., Bonardi, G., Colonna, V., Dietrich, D., Giunta, G., Ippolito, F., Liguori, V., Lorenzoni, P., Paglionico, A., Perrone, V., Piccarreta, G., Russo, M., Scandone, P., Zanettin-Lorenzoni, E., Zuppetta, A., 1976. L'Arco Calabro-Peloritano nell'orogene Appenninico-Maghrebide. Mem. Soc. Geol. It. 17, 1–60.

Andreani, L., Gloaguen, R., 2016. Geomorphic analysis of transient landscapes in the Sierra Madre de Chiapas and Maya Mountains (northern Central America): implications for the North American–Caribbean–Cocos plate boundary. Earth Surf. Dynam. 4, 71–102, doi:10.5194/esurf-4-71-2016.

Andreani, L., Stanek, K. P., Gloaguen, R., Krentz, O., Domínguez-González, L., 2014. DEM-based analysis of interactions between tectonics and landscapes in the Ore Mountains and Eger Rift (East Germany and NW Czech Republic). Remote Sensing 6, 7971–8001, doi:10.3390/rs6097971.

Antonioli, F., Dai Pra, G., Segre, A.G., Sylos Labin, S., 2004. New data on late Holocene uplift-rate in Calabria and Messina Straits area, Italy. Quat. Nova 8, 71–84.

Antonioli, F., Ferranti, L., Lambeck, K., Kershaw, S., Verrubbi, V., Dai Pra, G., 2006. Late Pleistocene to Holocene record of changing uplift-rates in southern Calabria and northeastern Sicily (southern Italy, Central Mediterranean Sea). Tectonophysics 422, 23–40, doi:10.1016/j.tecto.2006.05.003.

Ascione, A., Ciarcia, S., Di Donato, V., Mazzoli, S., Vitale, S., 2012. The Pliocene-Quaternary wedge-top basins of southern Italy: an expression of propagating lateral slab tear beneath the Apennines. Basin Research 24, 456–474, doi: 10.1111/j.1365-2117.2011.00534.x

Ascione, A., Cinque, A., 1999. Tectonics and erosion in the long-term relief history of the Southern Apennines (Italy). Zeitschrift fur Geomorphologie N.F. Suppl. Bd. 118, 1–16.

Balescu, S., Dumas, B., Guérémy, P., Lamothe, M., Lhénaff, R. Raffy, J., 1997. Thermoluminescence dating tests of Pleistocene sediments from uplifted marine shorelines along the southwest coastline of the Calabria Peninsula (southern Italy). Palaeog. Palaeocl. Palaeoecol., 130, 25-41, doi.org/10.1016/S0031-0182(96)00119-8.

Barrier, P., 1986. Évolution paléogeographique du détroit de Messine au Pliocène et au Pléistocène. Giornale di Geologia 3, 48, 7-24.

Berlin, M. M., Anderson, R. S., 2007. Modeling of knickpoint retreat on the Roan Plateau, western Colorado, J. Geophys. Res., 112, F03S06, doi:10.1029/2006JF000553.

Bianca, M., Catalano, S., De Guidi, G., Gueli, A.M., Monaco, C., Ristuccia, G.M., Stella, G., Tortoric,i G., Tortorici, L., Troja, S.O., 2011. Luminescence chronology of Pleistocene marine terraces of Capo Vaticano peninsula (Calabria, Southern Italy). Quat. Int. 231, 114-121, doi.org/10.1016/j.quaint.2010.07.013.

Bishop, P., Hoey, T.B., Jansen, J.D., Artza, I.L., 2005. Knickpoint recession rate and catchment area: the case of uplifted rivers in Eastern Scotland. Earth Surface Processes and Landforms 30, 767-778, 30, doi: 10.1002/esp.1191

Bookhagen, B., Strecker, M.R., 2012. Spatiotemporal trends in erosion rates across a pronounced rainfall gradient: examples from the southern central Andes. Earth Planet. Sci. Lett. 327–328, 97–110, doi:10.1016/j.epsl.2012.02.005.

Bonardi, G., Cavazza, W., Perrone, V., Rossi, S., 2001. Calabria-Peloritani terrane and Northern Ionian Sea. In: Vai, G.B., Martini, I.P. (eds), Anatomy of an Orogen: the Apennines and adjacent Mediterranean Basins. Kluwer Academic Publishers, Dordrecht, 287–306.

Bordoni, G., Valensise, G., 1998. Deformation of the 125-kamarine terrace in Italy: tectonic implications. In Stewart, I. S., Vita-Finzi, C., (eds) Coastal Tectonics, Geol. Soc. Lond. Spec. Publ. 146, 71–110.

Brancaccio, L., Cinque, A., Romano, P., Rosskopf, C., Russo, F., Santangelo, N., Santo, A., 1991. Geomorphology and neotectonic evolution of a sector of the Tyrrhenian flank of the Southern Apennines (Region of Naples, Italy). Zeitschrift für Geomorphologie N.F. 82, 47–58.

Calcaterra, D., Parise, M., 2010. Weathering in the crystalline rocks of Calabria, Italy, and relationships to landslides. In: Calcaterra, D., Parise, M., (eds): Weathering as a Predisposing Factor to Slope Movements. Geological Society, London, Engineering Geology Special Publications 23, 105–130.

Carbone, S., Messina, A., Lentini, F., 2008. Note illustrative delle Carta geologica d'Italia, Foglio 601 Messina_reggio Calabria. ISPRA, Servizio Geologico d'Italia, pp.179.

Catalano, S., Cinque, A., 1995. Dati preliminari sull'evoluzione neotettonica dei Peloritani settentrionali (Sicilia nord-orientale) sulla base dei dati morfologici. Studi Geologici Camerti, Volume Speciale 2, 113‑123.

Catalano, S., De Guidi, G., 2003. Late Quaternary uplift of northeastern Sicily: relation with the active normal faulting deformation. J. Geodyn. 36, 445–467, doi.org/10.1016/S0264-3707(02)00035-2.

Catalano, S., De Guidi, G., Monaco, C., Tortorici, L., 2003. Long-term behaviour of the Late Quaternary normal faults in the Strait of Messina region: structural and morphological constraints. Quat. Int. 101−102, 81–91, doi.org/10.1016/S1040-6182(02)00091-5.

Catalano, S., De Guidi, G., Monaco, C., Tortorici, G., Tortorici, L., 2008. Active faulting and seismicity along the Siculo–Calabrian Rift Zone (Southern Italy). Tectonophysics 453, 177–192, doi.org/10.1016/j.tecto.2007.05.008.

Catalano, S., Di Stefano, A., 1997. Sollevamento e tettogenesi Pleistocenica lungo il margine tirrenico dei Monti Peloritani: integrazione dei dati geomorfologici, strutturali e biostratigrafici. Il Quaternario, Italian Journal of Quaternary Science 10, 337‑342.

Cavazza, W., Dahl, J. 1990. Note on the temporal relationships between sandstone compaction and precipitation of authigenic minerals. Sed. Geol. 69, 37-44, doi.org/10.1016/0037-0738(90)90099-F.

Cavazza, W., DeCelles, P.G., 1993. Miocene submarine canyons and associated sedimentary facies in southeastern Calabria, southern Italy. Geol. Soc. Am. Bull. 105, 1297–1309, doi.org/10.1130/0016-7606(1993)105<1297:GOAMSC>2.3.CO;2.

Cavazza, W., DeCelles, P.G., 1998. Upper Messinian siliciclastic rocks in southeastern Calabria (southern Italy): paleotectonic and eustatic implications for the evolution of the central Mediterranean region. Tectonophysics 298, 223–241, doi.org/10.1016/S0040-1951(98)00186-3.

Cavazza, W., Ingersoll, R.V., 2005. Detrital modes of the Ionian forearc basin fill (Oligocene–Quaternary) reflect the tectonic evolution of the Calabria-Peloritani terrane (southern Italy). J. Sed. Res. 75, 268–279, doi.org/10.2110/jsr.2005.020.

Champagnac, J.D., Molnar, P., Sue, C., Herman, F., 2012. Tectonics, climate, and mountain topography. J. Geophys. Res. 117, B02403, doi:10.1029/2011JB008348

Chiarabba, C., De Gori, P., Speranza, F., 2008. The southern Tyrrhenian subduction zone: Deep geometry, magmatism and Plio-Pleistocene evolution. Earth and Planetary Science Letters 268, 408–423, doi.org/10.1016/j.epsl.2008.01.036.

Cifelli, F., Mattei, M., Della Seta, M., 2008. Calabrian Arc oroclinal bending: the role of subduction. Tectonics 27 (5), doi:10.1029/2008TC002272.

Cirrincione, R., Ortolano, G., Pezzino, A., Punturo, R., 2008. Poly-orogenic multi-stage metamorphic evolution inferred via P–T pseudosections: an example from Aspromonte Massif basement rocks (Southern Calabria, Italy). Lithos 103(3-4),466–502, doi.org/10.1016/j.lithos.2007.11.001.

Cosentino, D., Gliozzi, E., 1988. Considerazioni sulle velocità di sollevamento di depositi eutirreniani dell'Italia Meridionale e della Sicilia. Mem. Soc. Geol. It. 41, 653–665.

Critelli, S., Muto, F., Tripodi, V., 2016. Note illustrative delle Carta geologica d'Italia, Figlio 603 Bovalino. ISPRA, Servizio Geologico d'Italia, pp.108.

Critelli, S., Muto, F., Tripodi, V., 2017a. Note illustrative delle Carta geologica d'Italia, Figlio 615 Melito di Porto Salvo. ISPRA, Servizio Geologico d'Italia, pp.110.

Critelli, S., Muto, F., Tripodi, V., 2017b. Note illustrative delle Carta geologica d'Italia, Figlio 590 Taurianova. ISPRA, Servizio Geologico d'Italia, pp.116.

Cyr, A.J., Granger, D.E., Olivetti, V., Molin, P., 2010. Quantifying rock uplift rates using channel steepness and cosmogenic nuclide-determined erosion rates: examples from northern and southern Italy. Lithosphere 2, 188–198, doi.org/10.1130/L96.1.

Cyr, A.J., Granger, D.E., Olivetti, V., Molin, P., 2013. Distinguishing between tectonic and lithologic controls on bedrock channel longitudinal profiles using cosmogenic ^{10}Be erosion rates and channel steepness index. Geomorphology 209, 27–38, doi.org/10.1016/j.geomorph.2013.12.010.

D'Agostino, N., Selvaggi, G., 2004. Crustal motion along the Eurasia-Nubia plate boundary in the Calabrian Arc and Sicily and active extension in the Messina Straits from GPS measurements. J. Geophys. Res. 109, B11402, doi:10.1029/2004JB002998.

D'Arcy, M., Whittaker, A.C., 2014. Geomorphic constraints on landscape sensitivity to climate in tectonically active areas. Geomorphology, 204, 366-381, doi.org/10.1016/j.geomorph.2013.08.019.

Del Ben, A., Barnaba, C., Taboga, A., 2008. Strike-slip systems as the main tectonic features in the Plio-Quaternary kinematics of the Calabrian Arc. Mar. Geophys. Res. 29, 1–12, doi: 10.1007/s11001-007-9041-6.

De Rosa, R., R. Dominici, P. Donato, and D. Barca (2008), Widespread syn-eruptive volcaniclastic deposits in the Pleistocenic basins of South-Western Calabria, J. Volcanol. Geotherm. Res. 177, 155–169, doi.org/10.1016/j.jvolgeores.2007.11.011.

DiBiase, R.A.,Whipple, K.X., 2011. The influence of erosion thresholds and runoff variability on the relationships among topography, climate, and erosion rate. J. Geophys. Res. 116, F04036, doi.org/10.1029/2011JF002095.

DISS Working Group, 2015. Database of Individual Seismogenic Sources (DISS), Version 3.2.0: A Compilation of Potential Sources for Earthquakes Larger Than M 5.5 in Italy and Surrounding Areas. Istituto Nazionale di Geofisica e Vulcanologia, http://dx.doi.org/10.6092/INGV.IT-DISS3.2.0 (CC-BY NC SA). http://diss.rm.ingv.it/diss/.

Di Stefano, A., Longhitano, S., Smedile, A. 2007. Sedimentation and tectonics in a steep shallow-marine depositional system: stratigraphic arrangement of the Plio-Pleistocene Rometta succession (NE Sicily, Italy). Geol. Carpathica 58, 1, 71-87

Di Stefano, A., Longhitano, S., 2009. Tectonics and sedimentation of the Lower and Middle Pleistocene mixed siliciclastic/bioclastic sedimentary successions of the Ionian Peloritani Mts (NE Sicily, Southern Italy): the onset of opening of the Messina Strait. Central Eur. Journ. of Geosciences, 1(1), 33-62, doi.org/10.2478/v10085-009-0002-y.

Dumas, B., Gueremy, P., Hearty, P.J., R. Lhenaff, and J. Raffy 1988), Morphometric analysis and amino acid geochronology of uplifted shorelines in a tectonic region near Reggio Calabria, South Italy, Palaeogeogr., Palaeoclimatol., Palaeoecol., 68, 273– 289, doi.org/10.1016/0031-0182(88)90045-4.

Dumas, B., Gueremy, P., Lhenaff, R., Raffy, J., 2000. Périodicités de temps long et de temps court, depuis 400000 ans, dans l'étagement des terrasses marines en Calabre méridionale (Italie). Géomorphologie: relief, processus, environnement 1, 25-44.

Duvall, A., Kirby, E., Burbank, D.W., 2004. Tectonic and lithologic controls on bedrock channel profiles and processes in coastal California. J. Geophys. Res. 109. http:// dx.doi.org/10.1029/2003JF000086.

Faccenna, C., Becker, T.W., Lucente, F.P., Jolivet, L., Rossetti, F., 2001. History of subduction and back-arc extension in the Central Mediterranean. Geophys. J. Int. 145, 809–820, doi.org/10.1046/j.0956-540x.2001.01435.x.

Faccenna, C., Piromallo, C., Crespo-Blanc, A., Jolivet, L., Rossetti, F., 2004. Lateral slab deformation and the origin of the western Mediterranean arcs. Tectonics 23, TC1012, doi:10.1029/ 2002TC001488.

Ferranti, L., Antonioli, F., Mauz, B., Amorosi, A., Dai Prà, G., Mastronuzzi, G., Monaco, C., Orrù, P., Pappalardo, M., Radtke, U., Renda, P., Romano, P., Sansò, P., Verrubbi, V., 2006. Markers of the last interglacial sea-level high stand along the coast of Italy: tectonic implications. Quat. Int. 145–146, 30–54, doi.org/10.1016/j.quaint.2005.07.009.

Ferranti, L., Monaco, C., Antonioli,, F., Maschio, L., Kershaw, S., Verrubbi, V., 2007. The contribution of regional uplift and coseismic slip to the vertical crustal motion in the Messina Straits, Southern Italy: evidence from raised late Holocene shorelines. J. Geophys. Res. 112, B06401, doi:10.1029/2006JB004473

Ferranti, L., Monaco, C., Morelli, D., Antonioli, F., Maschio, L., 2008. Holocene activity of the Scilla Fault, Southern Calabria: Insights from coastal morphological and structural investigations. Tectonophysics 453, 74–93, doi.org/10.1016/j.tecto.2007.05.006.

Ghisetti, F., 1984. L'evoluzione strutturale del bacino plio-pleistocenico di Reggio Calabria nel quadro geodinamico dell'arco calabro. Boll. Soc. Geol. Ital., **100**, 433-466.

Ghisetti, F., 1992. Fault parameters in the Messina Straits (southern Italy) and relations with the seismogenic source, Tectonophysics, 210, 117–133, doi.org/10.1016/0040-1951(92)90131-O.

Gioia, D, Gallicchio, S., Moretti, M., Schiattarella, M., 2014. Landscape response to tectonic and climatic forcing in the foredeep of the southern Apennines, Italy: insights from Quaternary stratigraphy, quantitative geomorphic analysis, and denudation rate proxies Earth Surf. Process. Landforms 39, 814–835, doi: 10.1002/esp.3544.

Gioia, D., Martino, C., Schiattarella, M., 2011. Long- to short-term denudation rates in the southern Apennines: geomorphological markers and chronological constraints. Geologica Carpathica 62 (1), 27-41, doi: 10.2478/v10096-011-0003-1.

Greco, R., Sorriso-Valvo, M., Catalano, E., 2007. Logistic Regression analysis in the evaluation of mass movements susceptibility: The Aspromonte case study, Calabria, Italy. Engineering Geology 89, 47–56, doi.org/10.1016/j.enggeo.2006.09.006.

Gueguen, E., Doglioni, C., Fernandez, M., 1998. On the post-25 Ma geodynamic evolution of the western Mediterranean. Tectonophysics 298, 259–269, doi.org/10.1016/S0040-1951(98)00189-9.

Haviv, I., Enze, Y., Whipple, K.X., Zilberman, E., Matmon, A., Stone, J., Fifield, K.L., 2010. Evolution of vertical knickpoints (waterfalls) with resistant caprock: insights from numerical modeling. J. Geophys. Res. 115, F03028, doi:10.1029/2008JF001187.

Hayakawa, Y., Matsukura, Y., 2003. Recession rates of waterfalls in Boso Peninsula, Japan, and a predictive equation, Earth Surf. Processes Landforms 28, 675– 684, doi: 10.1002/esp.519

Hijmans, R.J., Cameron, S.E., Parra, J.L., Jones, P.G., Jarvis, A., 2005. Very high resolution interpolated climate surfaces for global land areas. Int. J. Climatol. 25, 1965–1978, doi:10.1002/joc.1276

Hoke, G. D., Isacks, B. L., Jordan, T. E., Blanco, N., Tomlinson, A. J., Ramezani, J., 2007. Geomorphic evidence for post-10 Ma uplift of the western flank of the central Andes 18°30′–22°S. Tectonics 26, TC5021, doi:10.1029/2006TC002082.

Howard, A.D., 1994. A detachment-limited model of drainage basin evolution. Water Resour. Res. 30, 2261–2285, doi.org/10.1029/94WR00757.

Howard, A.D., 1998. Long profile development of bedrock channels: Interaction of weathering, mass wasting, bed erosion, and sediment transport. In Tinkle, K., Wohl, E.E. (eds.), Rivers over rock: Fluvial processes in bedrock channels: American Geophysical Union Geophysical Monograph 107, 297–319, doi.org/10.1029/GM107p0297.

Howard, A.D., Kerby, G., 1983. Channel changes in badlands. Geol. Soc. Am. Bull. 94, 739–752, doi.org/10.1130/0016-7606(1983)94<739:CCIB>2.0.CO;2.

Howard, A.D., Seidl, M.A., Dietrich, W.E., 1994. Modeling fluvial erosion on regional to continental scales. J. Geophys. Res. 99, 13971–13986, doi.org/10.1029/94JB00744.

Ibbeken, H., Schleyer, R., 1991. Source and Sediment — A Case Study of Provenance and Mass Balance at an Active Plate Margin (Calabria, Southern Italy). Springer, Berlin, 286 pp.

ISIDe working group, 2016. version 1.0, https://doi.org/10.13127/ISIDe (CC-BY).

Kastens, K. A., Mascle, J., Party, O. L. S., 1988. ODP Leg 107 in the Tyrrhenian Sea: Insights into passive margin and backarc basin evolution, Geol. Soc. Am. Bull. 100, 1140–1156, doi:10.1130/0016-7606(1988)100<1140:OLITTS>2.3.CO;2.

Kirby, E., Johnson, C., Furlong, K., Heimsath, A.M., 2007. Transient channel incision along Bolinas ridge, California: evidence for differential rock uplift adjacent to the San Andreas fault. J. Geophys. Res. 112, F03S07, http://dx.doi.org/10.1029/2006JF000559.

Kirby, E., Whipple, K., 2001. Quantifying differential rock-uplift rates via stream profile analysis, Geology 29(5), 415–418, doi.org/10.1130/0091-7613(2001)029<0415:QDRURV>2.0.CO;2.

Kirby, E., Whipple, K.X., 2012. Expression of active tectonics in erosional landscapes. J. Struct. Geol. 44, 54–75, doi.org/10.1016/j.jsg.2012.07.009.

Kirby, E., Whipple, K.X., Tang, W., Chen, Z., 2003. Distribution of active rock uplift along the eastern margin of the Tibetan Plateau: inferences from bedrock channel longitudinal profiles. J. Geophys. Res 108 (B4), 2217, doi:10.1029/2001JB000861.

Le Pera. E., Sorriso-Valvo, M., 2000. Weathering and morphogenesis in a Mediterranean climate, Calabria, Italy. Geomorphology 34, 251–270, doi.org/10.1016/S0169-555X(00)00012-X.

Malinverno, A., Ryan, W.B.F., 1986. Extension in the Tyrrhenian Sea and shortening in the Apennines as result of arc migration driven by sinking of the lithosphere. Tectonics 5, 227–245, doi: 10.1029/TC005i002p00227.

Martino, C., Nico, G., Schiattarella, M., 2009. Quantitative analysis of InSAR Digital Elevation Models for identification of areas with different tectonic activity in southern Italy. Earth Surface Processes and Landforms 34, 3-15, doi.org/10.1002/esp.1681.

Mayer, L., 2000. Application of digital elevation models to macroscale tectonic geomorphology. In: Summerfield, M.A., (Ed.), “Geomorphology and Global Tectonics”, John Wiley and Sons, London, 15-27.

Minelli L., Faccenna C., 2010. Evolution of the Calabrian accretionary wedge (central Mediterranean) Tectonics 29, TC4004, doi:10.1029/2009TC002562.

Miyauchi, T., Dai Pra, G., Sylos Labini, S., 1994. Geochronology of Pleistocene marine terraces and regional tectonics in the Tyrrhenian coast of South Calabria, Italy. Il Quaternario, Italian Journal of Quaternary Science 7(1), 17–34.

Molin, P., Fubelli, G., Dramis, F., 2012. Evidence of tectonic influence on drainage evolution in an uplifting area: the case of northern Sila (Calabria, italy). Geogr. Fis. Dinam. Quat. 35, 49-60, doi 10.4461/GFDQ.2012.35.5

Molin, P., Pazzaglia, F.J., Dramis, F., 2004. Geomorphic expression of active tectonics in a rapidly-deforming forearc, Sila Massif, Calabria, southern Italy. Am. J. Sci. 304, 559–589, doi: 10.2475/ajs.304.7.559.

Monaco, C., Barreca, G., Di Stefano, A., 2017. Quaternary marine terraces and fault activity in the northern mainland sectors of the Messina Strait (southern Italy). Ital. J. Geosci. 136, 3, doi: 10.3301/IJG.2016.10.

Monaco, C., Tortorici, L., 2000. Active faulting in the Calabrian arc and eastern Sicily, J. Geodyn. 29, 407– 424, doi.org/10.1016/S0264-3707(99)00052-6.

Montuori, C., Cimini, G. B., Favali, P., 2007. Teleseismic tomography of the southern Tyrrhenian subduction zone: New results from seafloor and land recordings, J. Geophys. Res., 112, B03311, doi:10.1029/2005JB004114.

Neri, G., Barberi, G., Oliva, G., Orecchio, B., 2005. Spatial variations of seismogenic stress orientations in Sicily, south Italy, Phys. Earth Planet. Inter. 148(2–4), 75–191, doi:10.1016/j.pepi.2004.08.009.

Niemann, J.D., Gasparini, N.M., Tucker, G.E., Bras, R.L., 2001. A quantitative evaluation of Playfair's law and its use in testing long-term stream erosion models. Earth Surface Processes and Landforms 26, 1317-1332, doi: 10.1002/esp.272

Olivetti, V., Cyr, A.J., Molin, P., Faccenna, C., Granger, D.E., 2012. Uplift history of the Sila Massif, southern Italy, deciphered from cosmogenic ^{10}Be erosion rates and river longitudinal profile analysis. Tectonics 31, doi.org/10.1029/2011TC003037.

Ouimet, W.B., Whipple, K.X., Granger, D.E., 2009. Beyond threshold hillslopes: channel adjustment to base-level fall in tectonically active mountain ranges. Geology 37, 579–582. http://dx.doi.org/10.1130/G30013A.1.

Patacca, E., Sartori, R., Scandone, P., 1990. Tyrrhenian basin and Apenninic arcs. Kinematic relations since late Tortonian times. Mem. Soc. Geol. It. 45, 425–451.

Pérez-Peña, J.V., Azañón, J.M., Azor, A., Tuccimei, P., Della Seta, M., Soligo, M., 2009. Quaternary landscape evolution and erosion rates for an intramontane Neogene basin (Guadix–Baza basin, SE Spain). Geomorphology 106, 206–218, doi.org/10.1016/j.geomorph.2008.10.018.

Pezzino, A., Angì, G., Fazi, E., Fiannacca, P., Lo Giudice, A., Ortolano, G., Punturo, R., Cirrincione, R., De Vuono, E., 2008. Alpine metamorphism in the Aspromonte Massif: implications for a new framework for the southern sector of the Calabria–Peloritani orogen, Italy. Int. Geol. Rev. 50, 423–441, doi.org/10.2747/0020-6814.50.5.423.

Pirazzoli, P.A., Mastronuzzi, G., Saliege, J.F., Sansò, P., 1997. Late Holocene emergence in Calabria, Italy. Mar. Geol. 141, 61–70, doi.org/10.1016/S0025-3227(97)00057-1.

Piromallo, C., Morelli, A., 2003. P wave tomography of the mantle under the Alpine–Mediterranean area. J. Geophys. Res. 108 (B2), 2065. doi:10.1029/2002JB001757.

Pirrotta, C., Barbano, M.S., Monaco, C., 2016. Evidence of active tectonics in southern Calabria (Italy) by geomorphic analysis: the examples of the Catona and Petrace rivers. Ital. J. Geosci. 135 (1), 142-156, doi.org/10.3301/IJG.2015.20.

Polonia, A., Torelli, L., Gasperini, L., Mussoni, P., 2012. Active faults and historical earthquakes in the Messina Straits area (Ionian Sea). Nat. Hazards Earth Syst. Sci. 12, 2311–2328, doi:10.5194/nhess-12-2311-2012.

Robustelli, G., Muto, F., 2017. The Crati River basin: geomorphological and stratigraphical data for the Plio–Quaternary evolution of northern Calabria, South Apennines, Italy. Geologica Carpathica 68 (1), 68-79, doi: 10.1515/geoca-2017-0006.

Robustelli, G., Muto, F., Scarciglia, F., Spina, V., Critelli, S., 2005. Eustatic and tectonic control on Late Quaternary alluvial fans along the Tyrrhenian Sea coast of Calabria (south Italy). Quaternary Science Reviews 24 (18–19), 2101–2119, doi.org/10.1016/j.quascirev.2004.08.025.

Robustelli, G., Russo Ermolli, E., Petrosino, P, Jicha, B., Sardella, R., Donato, P. 2014. Tectonic and climatic control on geomorphological and sedimentary evolution of the Mercure basin, southern Apennines, Italy. Geomorphology, 214, 423-425, doi.org/10.1016/j.geomorph.2014.02.026.

Robustelli, G., Sorriso-Valvo, M., 2017. The Aspromonte Massif: a natural laboratory for Geomorphology. In Soldati, M., Marchetti M., (eds.), Landscapes and Landforms of Italy, World Geomorphological Landscapes, 431-441, doi 10.1007/978-3-319-26194-2_37.

Roda-Boluda, D.C., Whittaker, A.C., 2016. Normal fault evolution and coupled landscape response: examples from the Southern Apennines, Italy. Basin Research, 30 (1), 186–209, doi.org/10.1111/bre.12215

Roda-Boluda, D.C., Whittake,r A.C., 2017. Structural and geomorphological constraints on active normal faulting and landscape evolution in Calabria, Italy. Journal of the Geological Society of London, doi.org/10.1144/jgs2016-097.

Roe, G., Montgomery, D.R., Hallet, B., 2002. The effects of orographic precipitation variations on the concavity of steady-state river profiles. Geology 30, 143-146, doi.org/10.1130/0091-7613(2002)030<0143:EOOPVO>2.0.CO;2.

Rovida, A., Locati, M., Camassi, R., Lolli, B., Gasperini, P. (eds.), 2016. CPTI15, the 2015 Version of the Parametric Catalogue of Italian Earthquakes. Istituto Nazionale di Geofisica e Vulcanologia. http://doi.org/10.6092/INGV.IT-CPTI15.

Scarfì, L., Langer, H, Scaltrito, A., 2009. Seismicity, seismotectonics and crustal velocity structure of the Messina Strait (Italy) Physics of the Earth and Planetary Interiors 177, 65–78, doi.org/10.1016/j.pepi.2009.07.010.

Schiattarella, M., Di Leo, P., Beneduce, P., Giano, S.I., 2003. Quaternary uplift vs tectonic loading: a case study from the Lucanian Apennine, southern Italy. Quat. Int. 101–102, 239–251, doi.org/10.1016/S1040-6182(02)00126-X.

Schiattarella, M., Di Leo, P., Beneduce, P., Giano, S.I., Martino, C., 2006. Tectonically driven exhumation of a young orogen: an example from southern Apennines, Italy. In: Willett, S.D., Hoviu,s N., Brandon, M.T., Fisher D. (eds), Tectonics, climate, and landscape evolution, Geological Society of America, Special Paper 398, Penrose Conference Series, 371–385.

Schiattarella, M., Giano, S.I., Gioia, D., Martino, C., Nico, G., 2013. Age and statistical properties of the summit palaeosurface of southern Italy. Geografia Fisica e Dinamica Quaternaria 36, 289-302, doi 10.4461/GFDQ.2013.36.23.

Schoenbohm, L. M., Whipple, K. X., Burchfiel, B. C., Chen, L., 2004. Geomorphic constraints on surface uplift, exhumation, and plateau growth in the Red River region, Yunnan Province, China, Geol. Soc. Am. Bull., 116, 895–909, doi:10.1130/B25364.1.

Scicchitano, G., Lo Presti, V., Spampinato, C.R., Gasparo Morticelli, M., Antonioli, F., Auriemma, R., Ferranti, L., Monaco, C., 2011. Millstones as indicators of relative sea-level changes in northern Sicily and southern Calabria coastlines, Italy. Quat. Int. 232, 92-104, doi.org/10.1016/j.quaint.2010.08.019.

Seidl, M. A., Dietrich, W. E., 1992. The problem of channel erosion into bedrock, Catena Suppl. 23, 101– 124.

Serpelloni, E., Bürgmann, R., Anzidei, M., Baldi, P., Mastrolembo Ventura, B., Boschi, E., 2010. Strain accumulation across the Messina Straits and kinematics of Sicily and Calabria from GPS data and dislocation modelling. Earth and Planetary Science Letters 298, 347–360, doi.org/10.1016/j.epsl.2010.08.005.

Sklar, L., Dietrich, W. E. 1998. River longitudinal profiles and bedrock incision models: Stream power and the influence of sediment supply. In: Tinkler, K. J., Wohl, E. E., (eds), Rivers Over Rock: Fluvial Processes in Bedrock Channels, Geophys. Monogr. Ser.107, 237–260.

Sklar, L.S., Dietrich, W.E. 2001. Sediment and rock strength controls on river incision into bedrock. Geology 29, 1087–1090, doi.org/10.1130/0091-7613(2001)029<1087:SARSCO>2.0.CO;2.

Sklar, L., Dietrich, W.E., 2004. A mechanistic model for river incision into bedrock by saltating bed load. Water Resources Research 40, W06301, doi.org/ 10.1029/2003WR002496.

Sklar, L.S., Dietrich, W.E., 2006. The role of sediment in controlling steady state bedrock channel slope: implications of the saltation abrasion incision model. Geomorphology 82(1-2), 58 83, doi.org/10.1016/j.geomorph.2005.08.019.

Snyder, N. P., Whipple, K. X., Tucker, G. E., Merritts D. J., 2000. Landscape response to tectonic forcing: Digital elevation model analysis of stream profiles in the Mendocino Triple Junction region, northern California. Geol. Soc. Am. Bull. 112, 1250– 1263, doi.org/10.1130/0016-7606(2000)112<1250:LRTTFD>2.0.CO;2.

Sorriso-Valvo, M. Terranova, O., 2006. The Calabrian fiumara. Z. Geomorphol. NF 143, 105–121.

Spagnolo, M., Pazzaglia F. J., 2005. Testing the geological influences on the evolution of river profiles: a case from the northern Apennines, Italy. Geogr. Fis. Din. Quat. 28, 103-113.

Speranza, F., Mattei, M., Sagnotti, L., Grasso, F., 2000. Rotational differences between the northern and southern Tyrrhenian domains: Paleomagnetic constraints from the Amantea basin (Calabria, Italy). J. Geol. Soc. 157, 327–334, doi:10.1144/jgs.157.2.327.

Stock, J. D., Montgomery, D. R., 1999. Geologic constraints on bedrock river incision using the stream power law, J. Geophys. Res. 104, 4983– 4993, doi.org/10.1029/98JB02139.

Tarboton, D. G., Bras, R. L., Rodriguez-Iturbe, I., 1989. Scaling and elevation in river networks. Water Resour. Res., 25, 2037–2051, doi.org/10.1029/WR025i009p02037.

Thomson, S. N., 1994a. Fission track analysis of the crystalline basement rocks of the Oligo-Miocene late-orogenic extension and erosion. Tectonophysics 238, 331–352, doi:10.1016/0040-1951(94)90063-9.

Thomson, S. N., 1994b. Fission-track analysis and provenance studies in Calabrian Are sedimentary rocks, southern Italy. Journal of the Geological Society 151, 463-471, doi:10.1144/gsjgs.151.3.0463.

Thomson, S. N., 1998. Assessing the nature of tectonic contact using fission track thermochronology: An example from the Calabrian Arc, southern Italy. Terra Nova, 10, 32–36, doi:10.1046/j.1365-3121.1998.00165.x.

Tortorici, L., Monaco, C., Tansi, C., Cocina, O., 1995. Recent and active tectonics in the Calabrian Arc (southern Italy). Tectonophysics 243, 37–55, doi.org/10.1016/0040-1951(94)00190-K.

Tripodi, V., Muto, F., Critelli, S., 2013. Structural style and tectono-stratigraphic evolution of the Neogene - Quaternary Siderno Basin, southern Calabrian Arc, Italy. Int. Geol. Rev. 55, 468–481, doi.org/10.1080/00206814.2012.723859.

Tripodi, V., Muto, F., Critelli, S., 2018. Neogene-Quaternary evolution of the forearc and backarc regions between the Serre and Aspromonte Massifs, Calabria (southern Italy). In press, https://doi.org/10.1016/j.marpetgeo.2018.03.028.

Tucker, G.E., Whipple, K.X., 2002. Topographic outcomes predicted by stream erosion models: sensitivity analysis and intermodel comparison. J. Geophys. Res. 107, doi: 10.1029/2001JB000162.

Valensise, G., Pantosti, D., 1992. A 125 kyr-long geological record of seismic source repeatability: the M.S.s (southern Italy) and the 1908 earthquake (MS 7 1/2). Terra Nova 4, 472–483, doi.org/10.1111/j.1365-3121.1992.tb00583.x.

Van Dijk, J.P., Scheepers, P.J.J., 1995. Neotectonic rotations in the Calabrian Arc; implications for a Pliocene-recent geodynamic scenario for the Central Mediterranean. Earth Sci Rev 39, 207–246, doi.org/10.1016/0012-8252(95)00009-7.

Wegmann, K.W., Pazzaglia, F.J., 2009. Late Quaternary fluvial terraces of the Romagna and Marche Apennines, Italy: climatic, lithologic, and tectonic controls on terrace genesis in an active orogen. Quat. Sci. Rev. 28, 137–165, doi.org/10.1016/j.quascirev.2008.10.006.

Westaway, R., 1993. Quaternary uplift of Southern Italy. J. Geophys. Res. 98, 21741–21772, doi.org/10.1029/93JB01566.

Whipple, K. X., 2004. Bedrock rivers and the geomorphology of active orogen, Annu. Rev. Earth Planet. Sci. 32, 151–185, doi:10.1146/ annurev.earth.32.101802.120356.

Whipple, K. X. (2001), Fluvial landscape response time: how plausible is steady state denudation?, Am. J. Sci., 301, 313-325, doi:10.2475/ajs.301.4-5.313.

1 Figure Captions

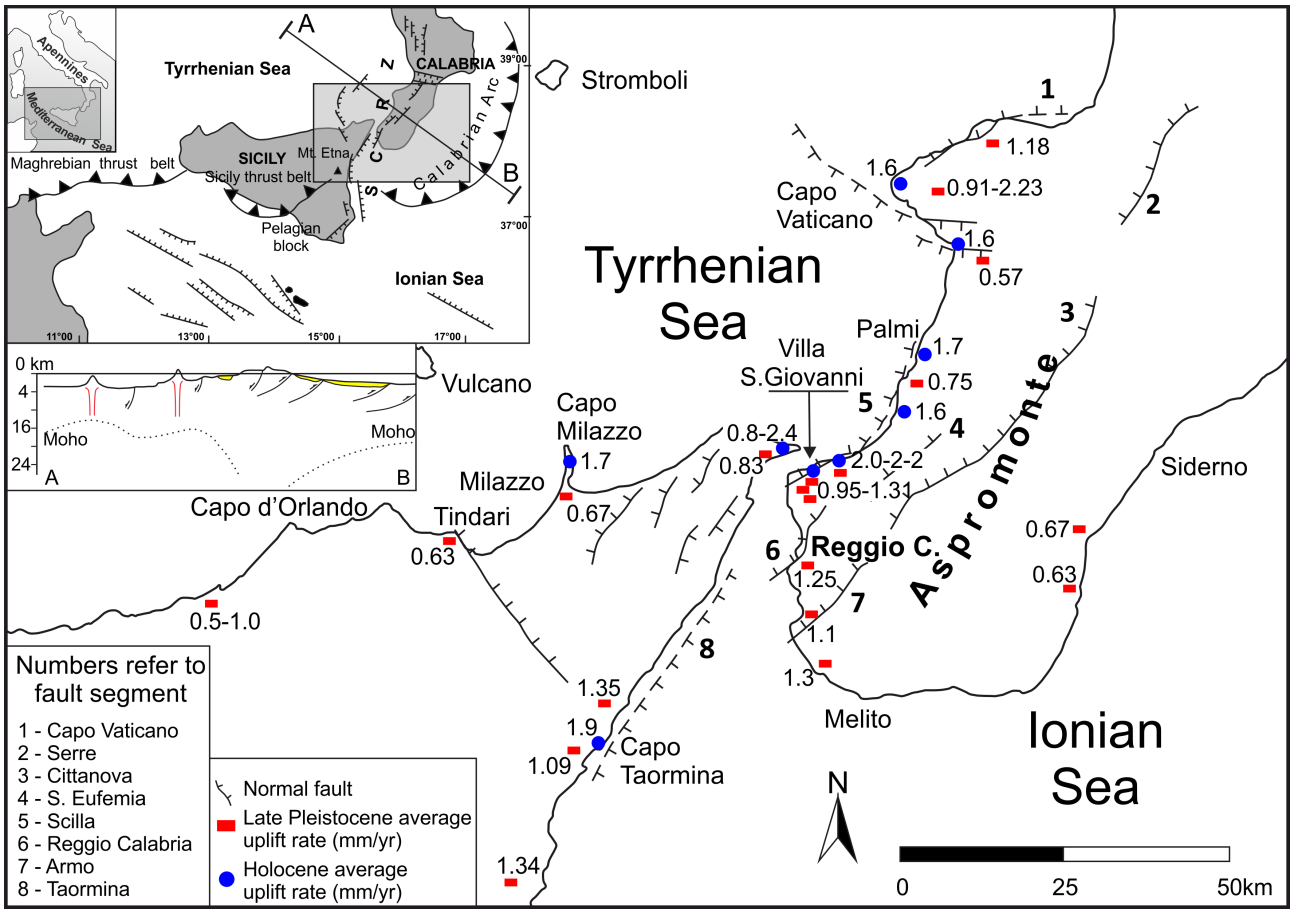

2

3 Fig. 1 - Tectonic sketch map of southern Calabria and northeastern Sicily (after Scicchitano et al., 2001; modified): its
4 location in the western Mediterranean framework and crustal thickness along a NW-SE profile across central Calabria
5 (top insets). The map shows the Quaternary fault segments of the Siculo-Calabrian rift zone and Late Pleistocene-
6 Holocene uplift rates.

7

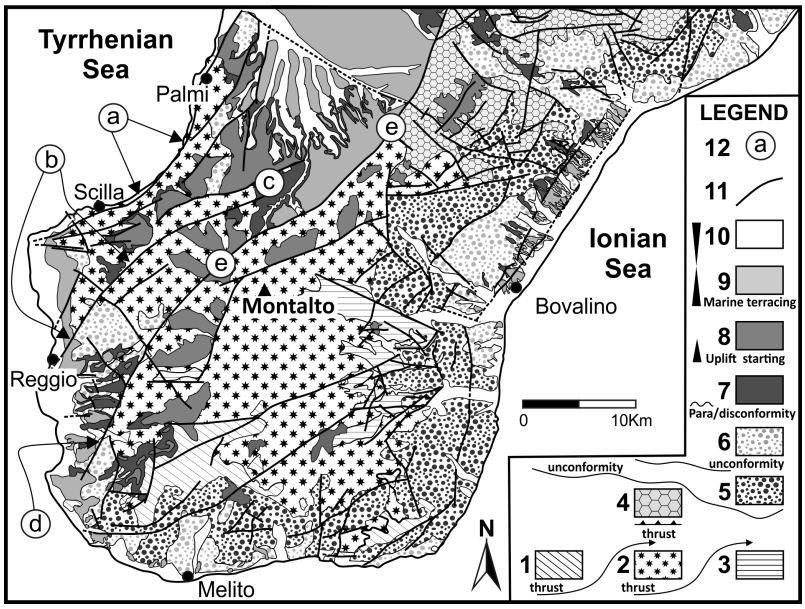

Fig. 2 - Geological sketch map of Aspromonte. (1) Stilo Unit. (2) Aspromonte Unit. (3) Lower Metapelite Unit. (4) Serre Unit. (5) Late Oligocene-Miocene sediments. (6) Late Miocene-Zanclean sediments. (7) Calcareniti di Vinco Formation. (8) late Early Pleistocene clastic deposits. (9) Middle Pleistocene sediments (Marine terraced and fluvial-deltaic deposits). (10) Late-Pleistocene-Holocene marine and fluvial deposits. (11) Fault segment. (a) Scilla fault. (b) Reggio Calabria-Calanna fault. (c) S.Eufemia fault. (d) Armo fault. (e) Cittanova-Delianuova fault (fault segments after Tortorici et al. (1995) and Catalano et al. (2008); modified).

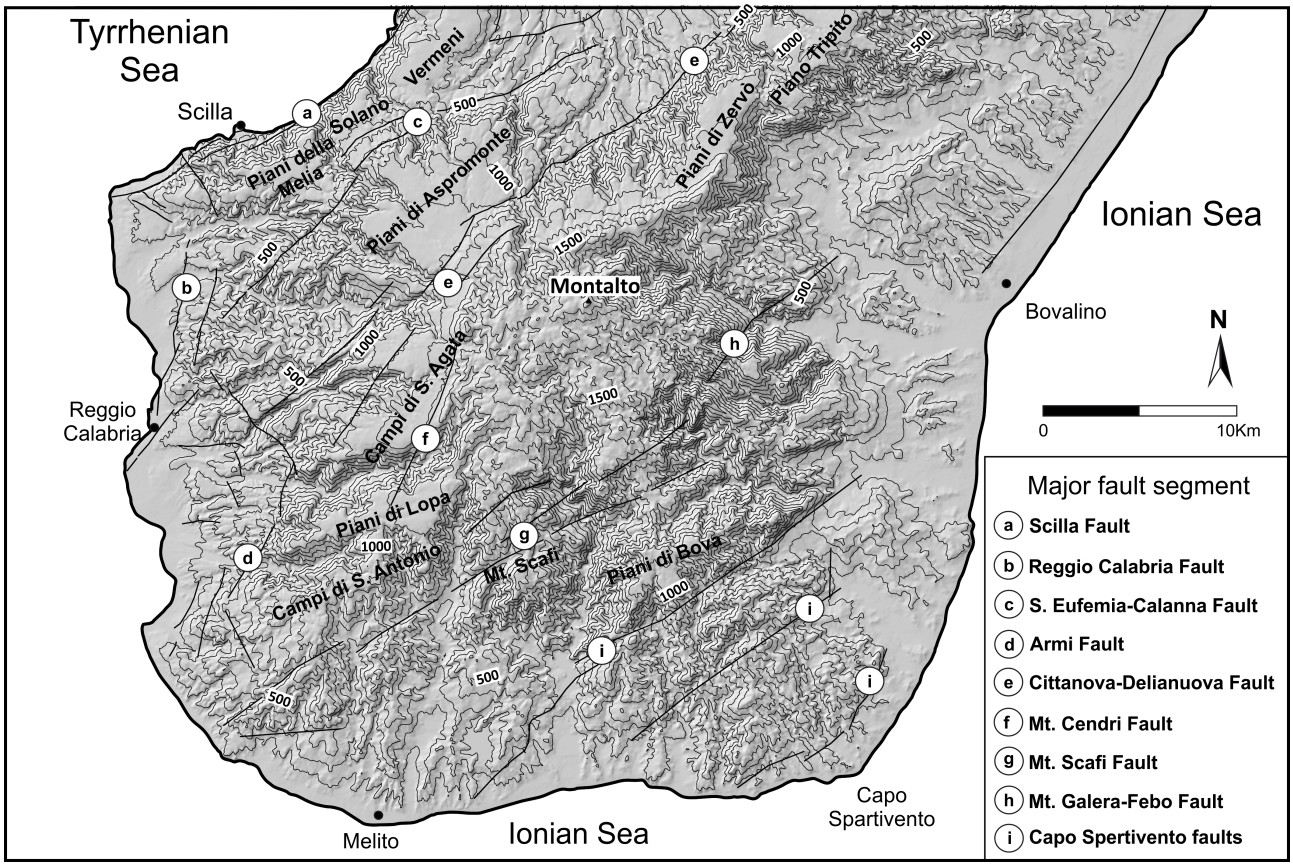

Fig. 3 – Hillshade and 100 m contour maps indicating the main relics of low-relief landsurfaces of the Aspromonte Massif. Their step-like distributed pattern is linked to the activity of fault segments of the Siculo-Calabrian rift zone (after DISS Working Group, 2015; ISIDe working group, 2016; Rovida et al., 2016; modified)

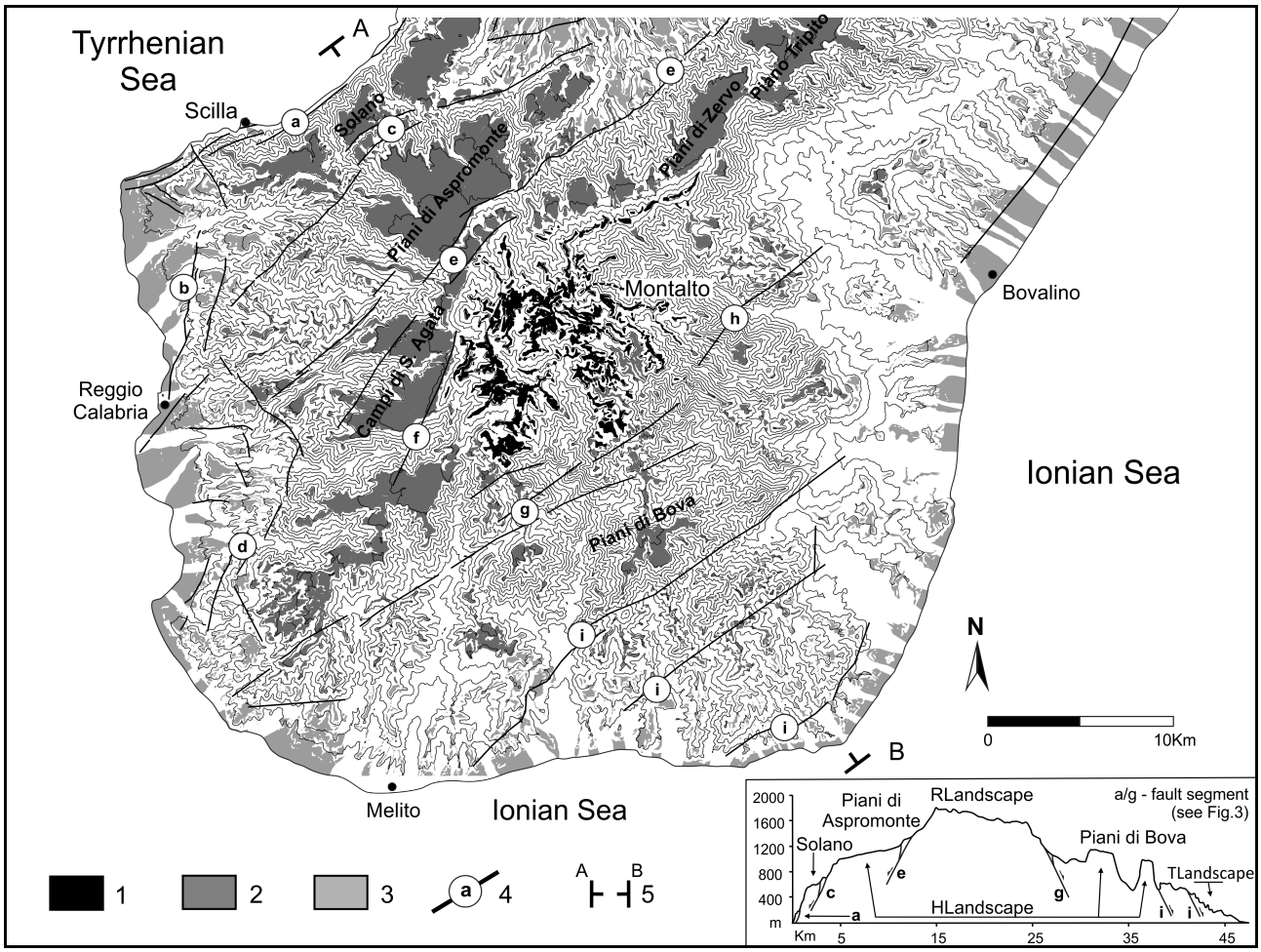

Fig. 4 - Topographic map of the Aspromonte Massif (100 m contour interval). The landscape is characterised by a stair of Late Plliocene-Quaternary landsurfaces representing the geomorphic response to the interaction among relief-smoothing processes (Relict and Hanging Landscapes; 1 and 2), Middle-Late Quaternary sea level changes (Terraced Landscape; 3) and tectonic uplift experienced by the study area. A NW-SE profile across the massif showing the active fault system of the Siculo–Calabrian Rift Zone and the distribution of the three orders of landsurfaces (bottom inset). (1) Relict Landscape. (2) Hanging Landscape. (3) Terraced Landscape. (4) Fault segment (see Fig. 3). 5) Trace of NW-SE topographic profile.

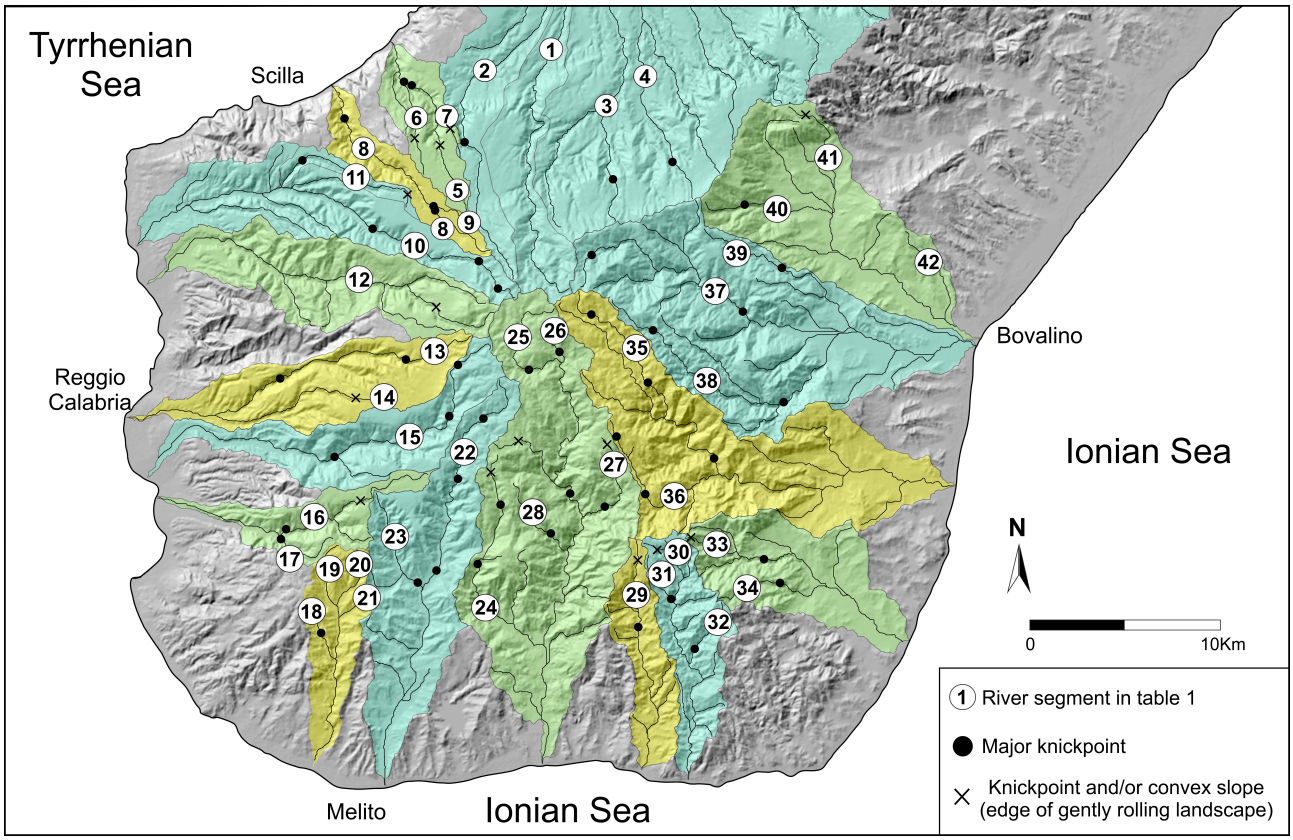

Fig. 5 – Hillshade map of the Aspromonte Massif showing channels examined in this study and the distribution of knickpoints. Identification numbers are keyed to Table 1. Areas shaded in blue, green and yellow refer to the major drainage basins.

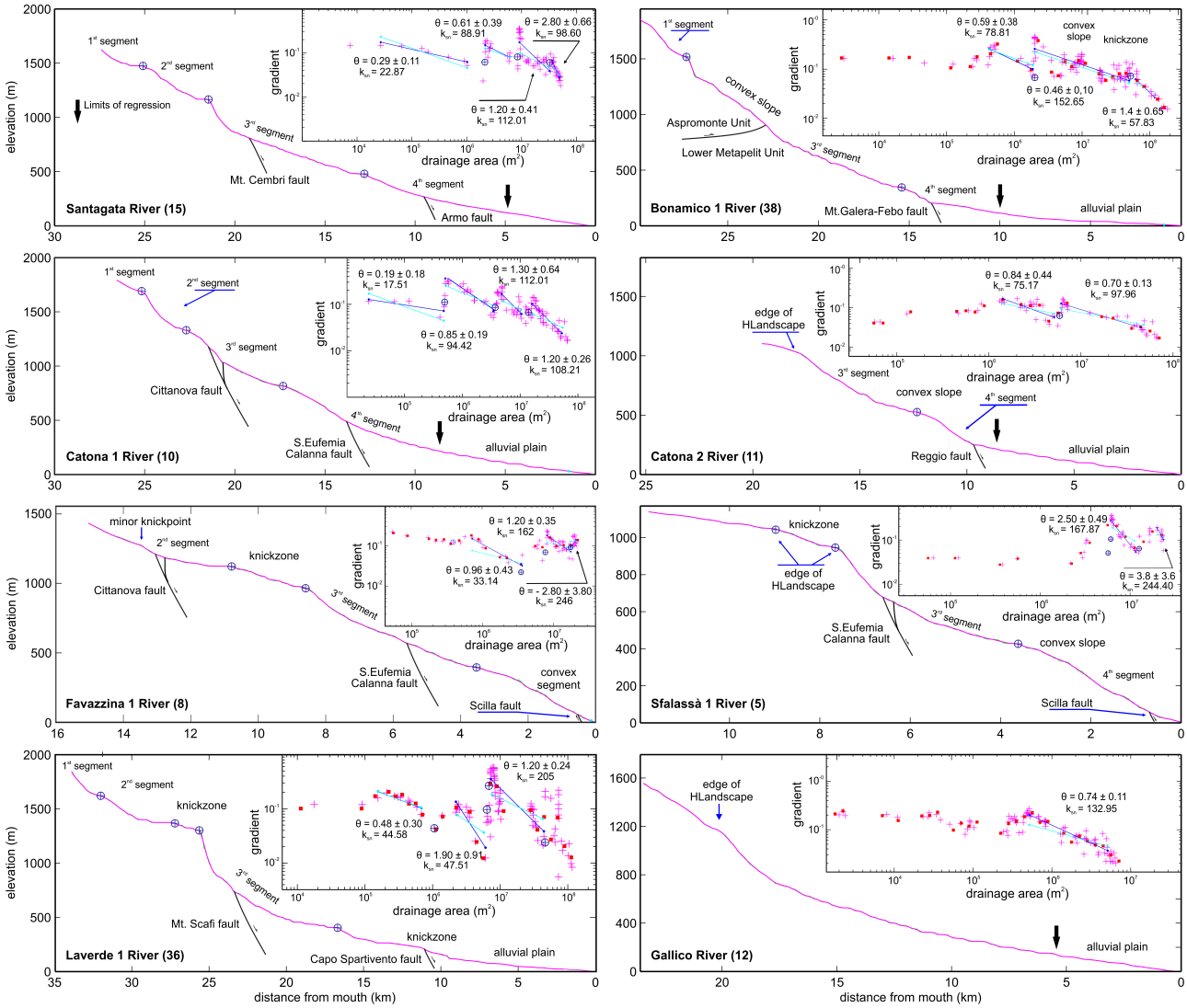

Fig. 6 - Longitudinal profiles and gradient-area data for selected rivers in Aspromonte. Gradients are plotted against upstream area for each channel (insets). The main channel segment of river profiles is also shown.

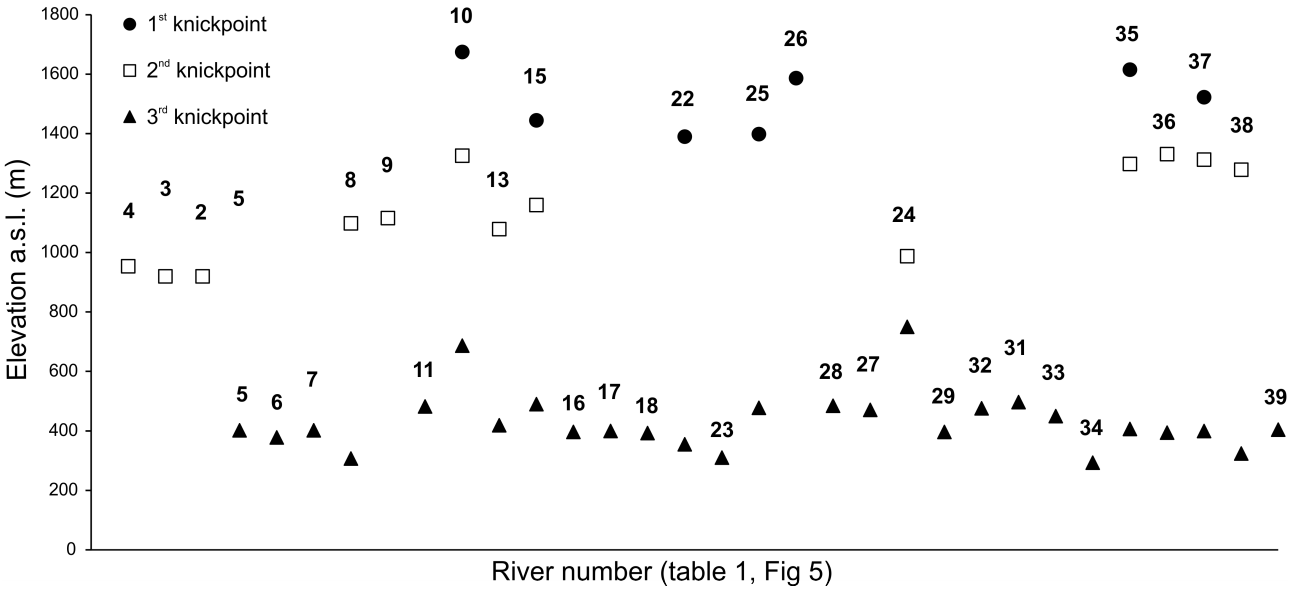

Fig. 7 - Elevation of the knickpoints from each river analyzed are plotted from the Northwest to the Southeast. The 1st (filled circle) and 2nd (square) knickpoint mark the edge of the low-relief surface atop Aspromonte (RLandscape) and HLandscape, respectively. The 3rd knickpoint (filled triangle) mark the inner edge of Terraced Landscape developed since Middle Pleistocene.

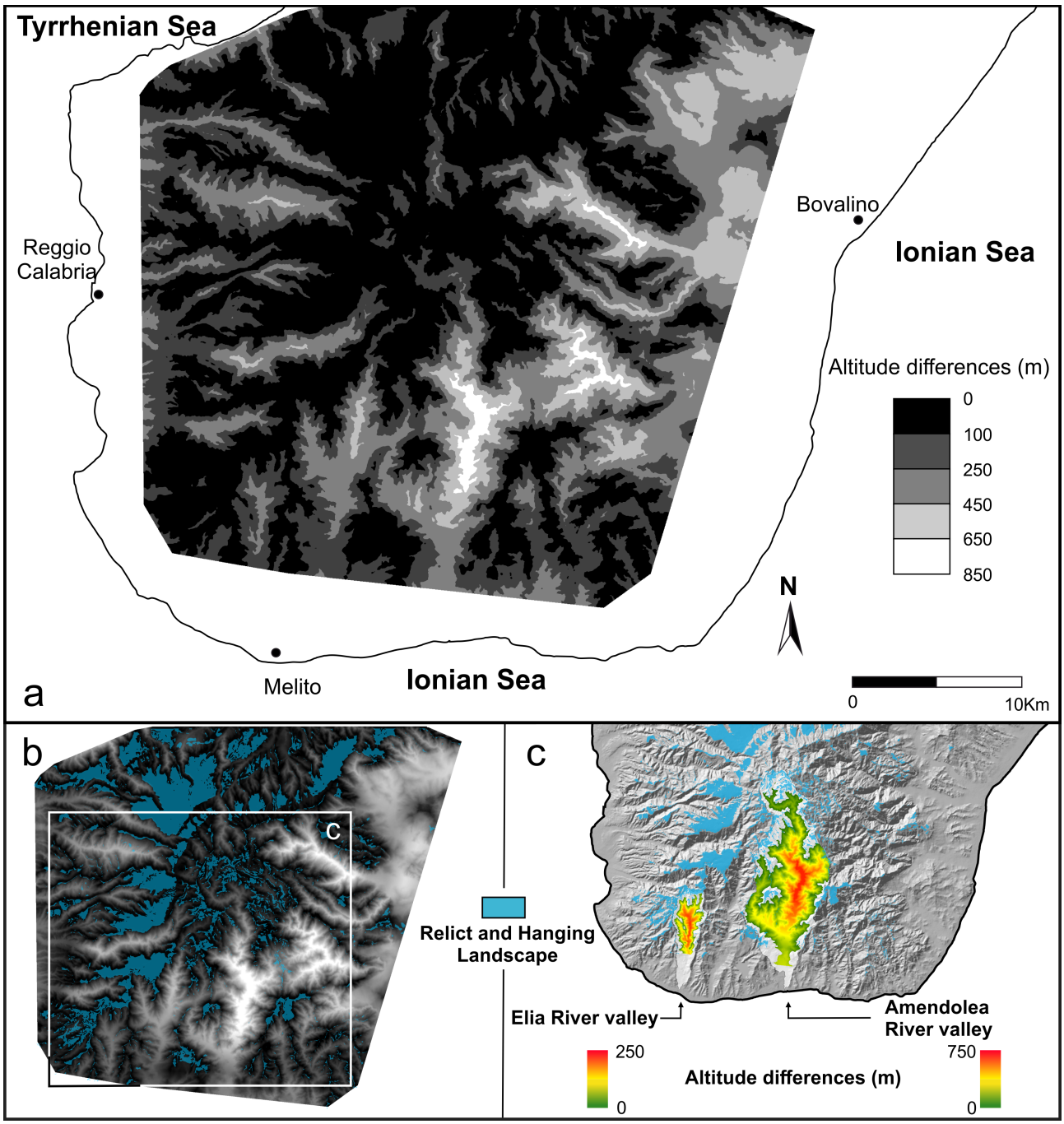

Fig. 8 – (a) Elevation differences between the reconstructed and the DEM topography. Note how the amount of erosion is low in the high-standing low-relief landsurfaces, whereas high values of erosion concentrate along the incised fluvial valleys on the Aspromonte massif flanks. Removal of low-relief surfaces by applying a 100m buffer to the edge of Relict

(R) and Hanging (H) Landscape (b) results in an increase of denudation rate up to 0.80 mm/yr^{-1} for the Amendolea River (c).

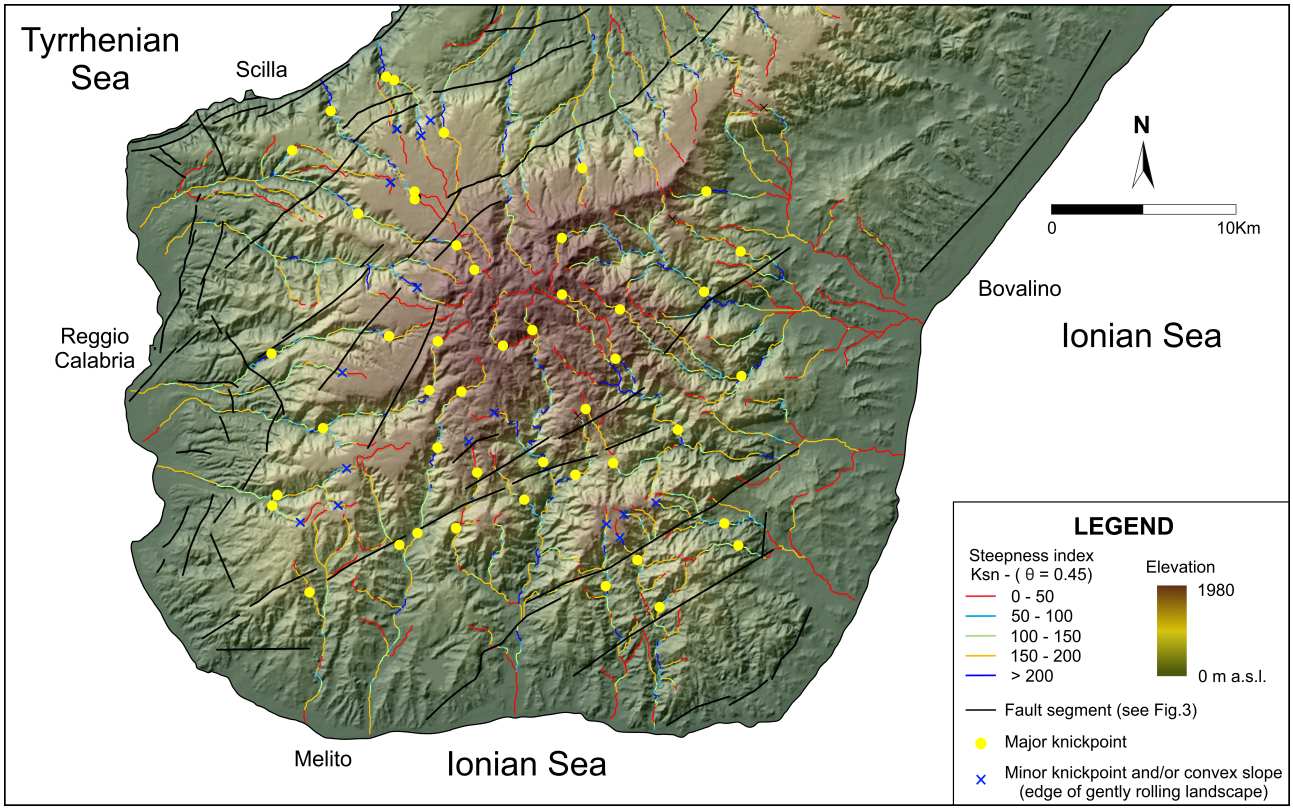

Fig. 9 - Map of steepness index (k_{sn}) values of all rivers analyzed in the Aspromonte Massif, generated automatically according to the operating procedures of Whipple et al. (2007). Yellow dots indicate major knickpoint locations. A large region of low k_{sn} values located in the central region of the map matches the rolling topography of the perched landscapes, limited by minor knickpoint and/or convex slope (blue crosses). Tectonic features from DISS Working Group (2015), ISIDe working group (2016), and Rovida et al. (2016). Note the high steepness indices adjacent to the edge of landsurfaces, and narrow belts of higher k_{sn} where rivers cross active normal faults.

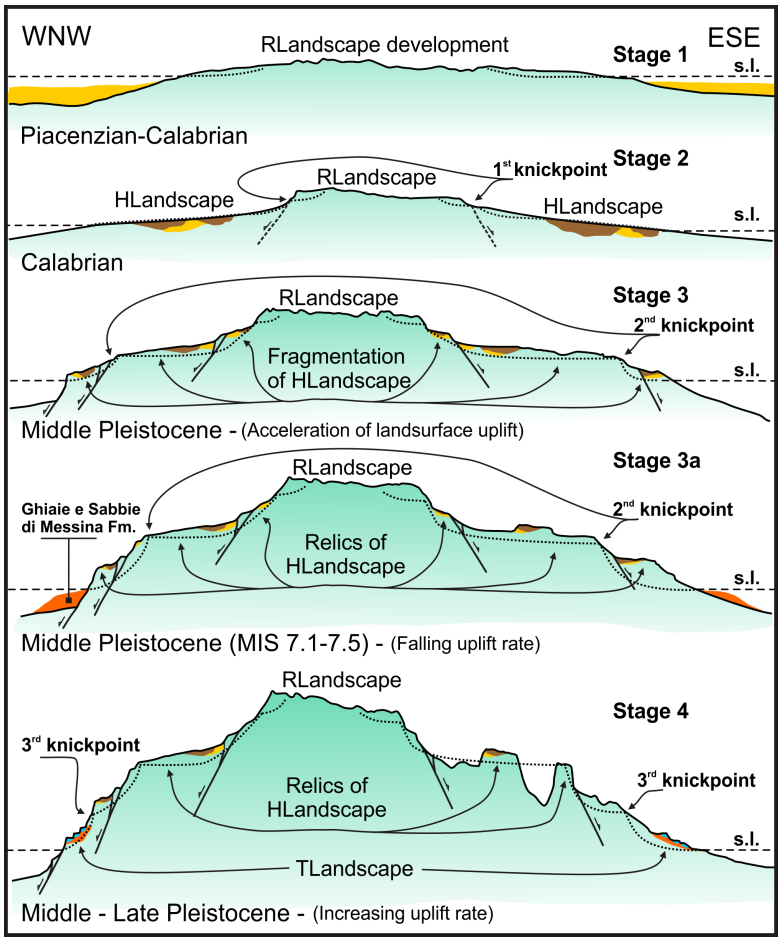

Fig. 10 – Schematic profiles of morpho-tectonic scenarios of the Aspromonte Massif resulting in three-phase incision. Evolutionary stages show the uplift history of the massif. Stage 1 – Low-relief landsurface (RLandscape) develop through fluvial-denudational relief smoothing processes during a long lasting period of slow uplift balanced by erosion. Crystalline rocks of the Aspromonte provide sediment supply for the Calcareniti di Vinco Fm.. Stage 2 - HLandscape development; Calabrian clastic deposits rest erosively on the Calcareniti di Vinco Fm and locally blanket the HLandscape. Changing scenario during the Middle Pleistocene: the ESE–WNW trending regional extension allows the development of the Siculo-Calabrian Rift Zone (Tortorici et al., 1995) responsible for the fragmentation of previous landscapes. Pulses of rapid uplift (Middle-Late Pleistocene) are directly translated to river morphology leading to the development of the 2nd and 3rd first knickpoint. First increase in uplift rate (Stage 3) causes channels to adjusts to plateau uplift by changing their gradient and dissecting low-relief landsurfaces (Stage 3a); Falling uplift rate produces a highly concave channel profile (middle segment) and sets out the conditions for the deposition of the Ghiaie e Sabbie di Messina Fm. (Carbone et al., 2007). Second increase in uplift rate (Stage 4) leads to the formation of the 3rd knickpoint. The rectilinear to convex profiles of lower segment in the NW suggest an imbalance between uplift and erosion (see text for details).

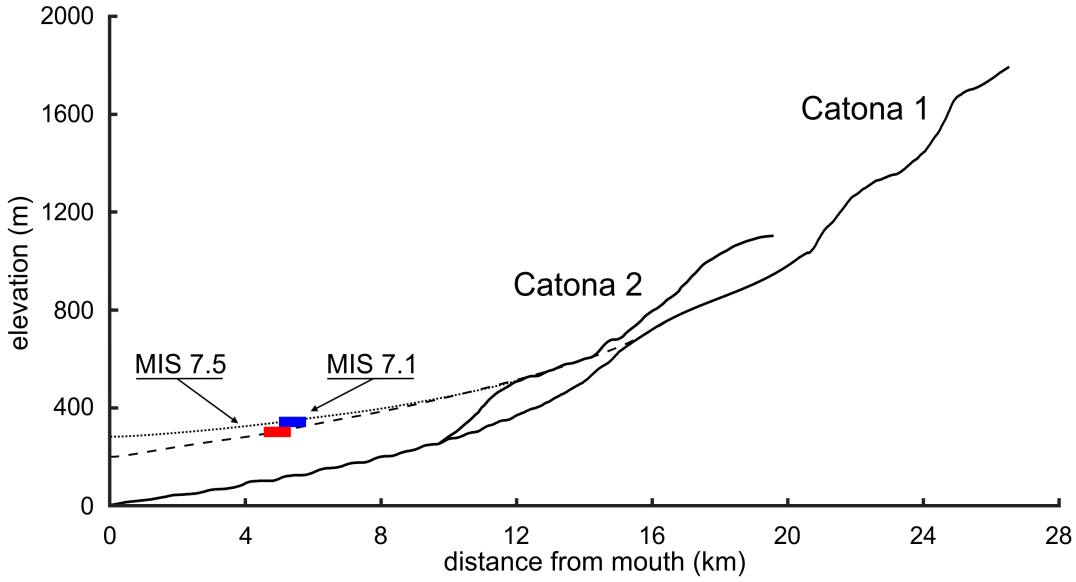

Fig. 11 – Relationship between elevation of the MIS 7.1-7.5 marine terraces (Monaco et al., 2017) and modeled middle channel segments of Catona 1 (dashed line) and Catona 2 (dotted line) rivers. The modeled profiles are reconstructed using interpolation of the slope–distance relationship from segments above knickpoints (e.g. Andreani et al., 2014; Andreani and Gloaguen, 2016).

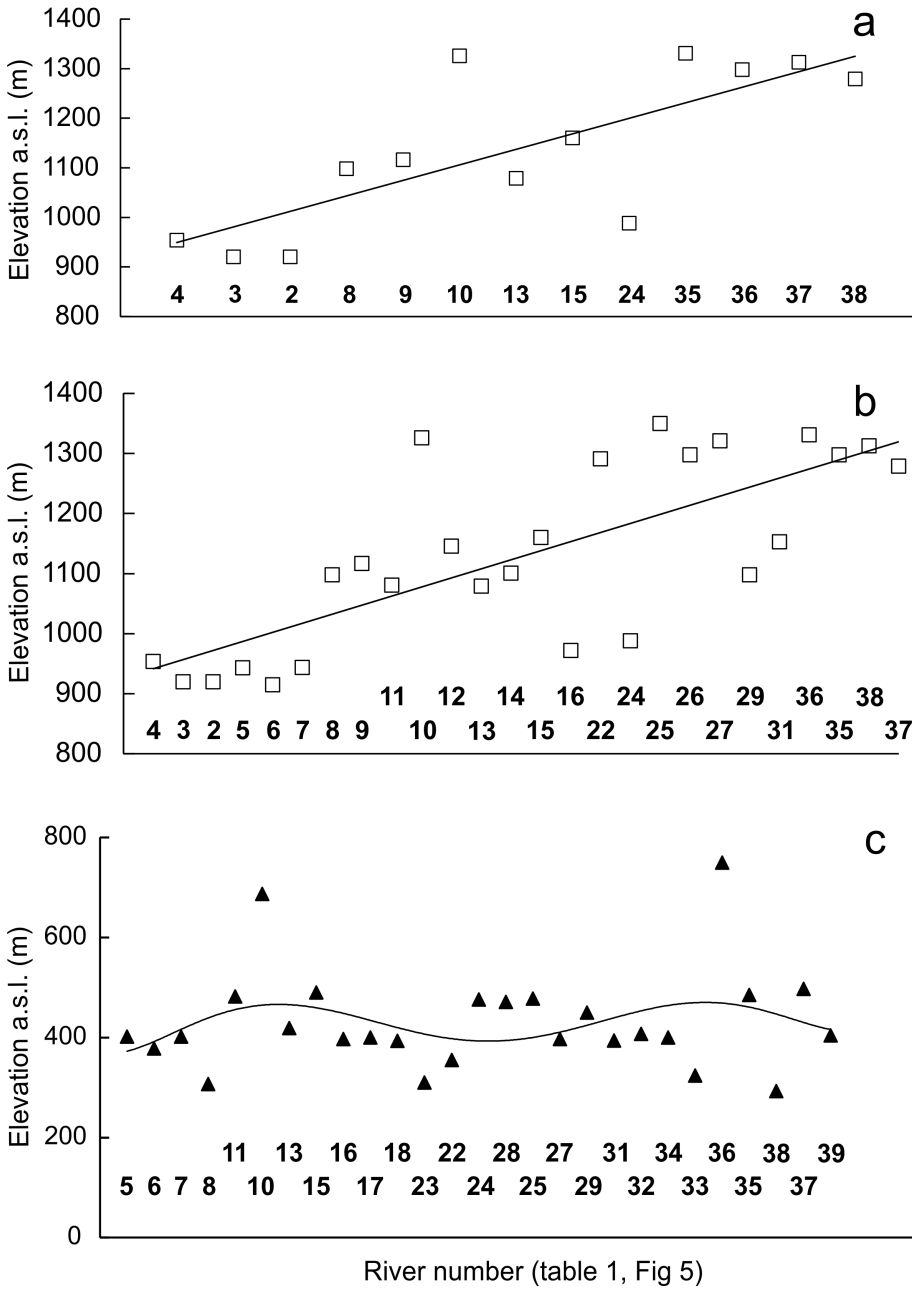

Fig. 12 – Elevation of the 2nd and 3rd knickpoints from each river analyzed. Elevation of major knickpoints (a) are supplemented by minor knickpoints (b) that mark the edge of the HLandscape. Both plots in (a) and (b) show linear regression through all data points (correlation coefficient ~ 0.6). This pattern may indicate the key role of rock strength and drainage area on knickpoint distribution. An undulatory pattern characterizes the distribution of 3rd knickpoint elevations (c); differential uplift is believed to be the key factor influencing its distribution.